

Manuscript Number: ECM-D-14-02029R2

Title: Design guidelines for H-Darrieus wind turbines: optimization of the annual energy yield

Article Type: Original research paper

Section/Category: 4. Clean Energy and Sustainability

Keywords: Darrieus, VAWT, wind turbine, design, energy yield, aerodynamics

Corresponding Author: Dr. Lorenzo Ferrari, Ph.D.

Corresponding Author's Institution: National Council of Research of Italy

First Author: Alessandro Bianchini, Ph.D.

Order of Authors: Alessandro Bianchini, Ph.D.; Giovanni Ferrara, Ph.D.; Lorenzo Ferrari, Ph.D.

Abstract: H-Darrieus wind turbines are gaining popularity in the wind energy market, particularly as they are thought to represent a suitable solution even in unconventional installation areas. To promote the diffusion of this technology, industrial manufacturers are continuously proposing new and appealing exterior solutions, coupled with tempting rated-power offers. The actual operating conditions of a rotor over a year can be, however, very different from the nominal one and strictly dependent on the features of the installation site. Based on these considerations, a turbine optimization oriented to maximize the annual energy yield, instead of the maximum power, is thought to represent a more interesting solution. With this goal in mind, 21600 test cases of H-Darrieus rotors were compared on the basis of their energy-yield capabilities for different annual wind distributions in terms of average speed. The wind distributions were combined with the predicted performance maps of the rotors obtained with a specifically developed numerical code based on a Blade Element Momentum (BEM) approach. The influence on turbine performance of the cut-in speed was accounted for, as well as the limitations due to structural loads (i.e. maximum rotational speed and maximum wind velocity). The analysis, carried out in terms of dimensionless parameters, highlighted the aerodynamic configurations able to ensure the largest annual energy yield for each wind distribution and set of aerodynamic constraints.

Florence, July 21st 2014

Dear Prof. Al-Nimr,

the importance to focus on the energy yield rather than on the rated power does not come as a surprise to the wind energy community. Several industrial manufacturers and even final customers, however, often perceive the rated power as the indicator of the quality of a small rotor.

This approach is particularly critical in small and medium size applications, where scale effects take place and a rotor optimized for a too high wind speed can indeed have a very poor performance for the largest part of the year, with a sensible detriment of the energy harvesting. This phenomenon is indeed emphasized in new installations contexts (e.g. a complex terrain or a built environment), which are thought to be the frontiers for a wider diffusion of wind turbines.

In the study we are submitting, an H-Darrieus turbines optimization oriented to maximize the annual energy yield is presented. Based on this approach, many study cases were analyzed and the best values for the main design parameters were highlighted with respect to the attended average wind speed in the installation site.

We would be very pleased if you could consider the paper for publication in “Energy Conversion and Management”.

Looking forward to hearing from you, best regards.

Alessandro Bianchini
Giovanni Ferrara
Lorenzo Ferrari

Energy Conversion and Management Submission Checklist

Please save a copy of this form to your computer, complete and upload as ‘Checklist for New Submissions’.

Your manuscript will be considered incomplete unless all the below requirements have been met. Please initial each step to confirm.

(1) I Lorenzo Ferrari confirm that the work described has not been published previously (except in the form of an abstract or as part of a published lecture or academic thesis), that it is not under consideration for publication elsewhere, that its publication is approved by all authors and that, if accepted, it will not be published elsewhere in the same form, in English or in any other language, without the written consent of the Publisher.

Authors found to be deliberately contravening the submission guidelines on originality and exclusivity shall not be considered for future publication in this journal.

(2) The source document is editable, i.e. Word, WordPerfect or Latex
LF

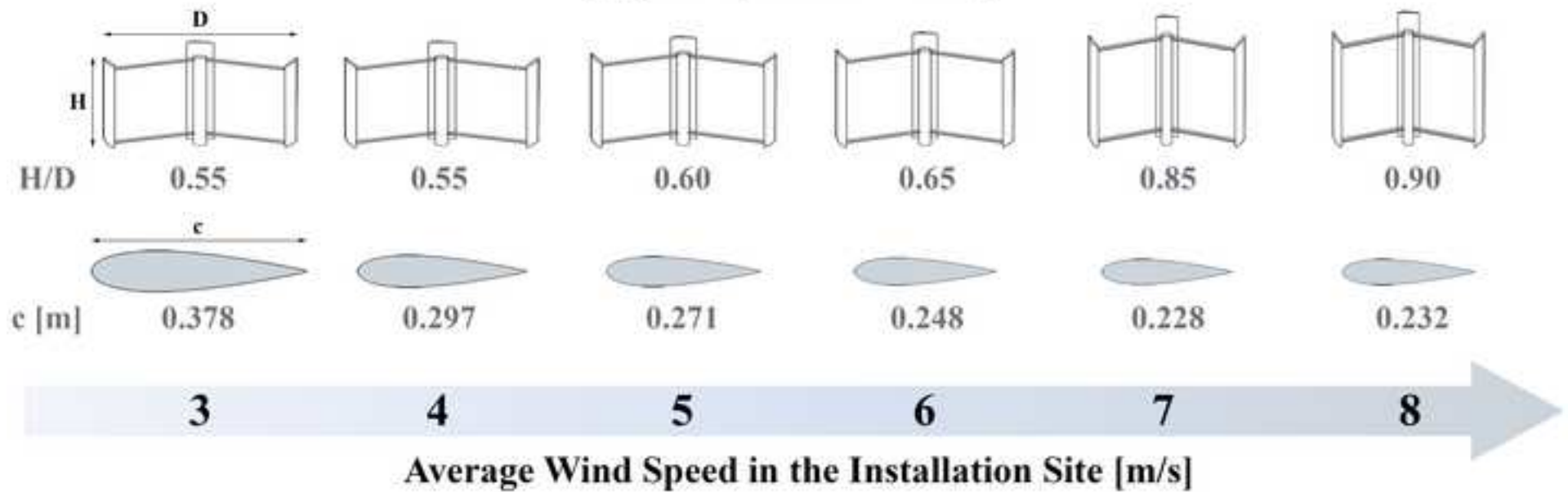
(3) The source document is double-spaced
LF

(4) The source document has been prepared prepared in 12 or 10 point font size, preferably 12 points
LF

(5) The source document is in one column per page
LF

(6) The figures and tables have been supplied: either integrated with the text file or as separate files.
LF

Optimized design based on a maximized energy-yield (e.g. Swept Area = 4 m²)



Research highlights

- Proposal for a new design criterion for H-Darrieus turbine based on the energy-yield maximization
- 21600 design cases analyzed to identify the best solutions for each installation site (i.e. average wind speed)
- Critical analysis of the best design choices in terms of turbine shape, dimensions, airfoils and constraints
- Notable energy increase provide by the proposed design approach
- Each site requires a specific turbine concept to optimize the energy yield

23 The wind distributions were combined with the predicted performance maps of the rotors
24 obtained with a specifically developed numerical code based on a Blade Element Momentum
25 (BEM) approach. The influence on turbine performance of the cut-in speed was accounted for,
26 as well as the limitations due to structural loads (i.e. maximum rotational speed and maximum
27 wind velocity). The analysis, carried out in terms of dimensionless parameters, highlighted the
28 aerodynamic configurations able to ensure the largest annual energy yield for each wind
29 distribution and set of aerodynamic constraints.

30 **Keywords**

31 Darrieus, VAWT, wind turbine, design, energy yield, aerodynamics

32 **1. Introduction**

33 In 2011, the wind energy market grew by 6% compared to 2010, despite the economic and
34 political turmoil in Europe and North America, with a newly installed power of 40.5 GW [1].

35 The great bulk of installed wind energy plant is today in the form of large wind farms [2]
36 which mainly comprehend large Horizontal Axis Wind Turbines (HAWTs) feeding into power
37 supply grids: turbines are becoming more and more efficient and a scale-up tendency is clearly
38 distinguishable. Moreover, technological improvements in design and efficient maintenance
39 have considerably reduced their operating cost and consequently disclosed new diffusion
40 frontiers like the offshore applications [3-4]. Whereas these installations are a valuable addition
41 to the grid capacity, they actually do not benefit people who are not served by grids. As a
42 consequence, much interest is being paid to understand where wind turbines can effectively
43 represent an alternative for delocalized power production [5-6]. Paradoxically, however, there
44 has been very little research and commercial development in the second part of the century on
45 small stand-alone systems, although great improvements in the blade aerodynamic design have
46 been made. In recent times, a reversal of this trend has been fortunately experienced.

47 Increasing interest is especially being paid by architects, project developers and local
48 governments to understand where small wind turbines can effectively be exploited to provide
49 delocalized power in the built environment (e.g. see Refs. [7-12]). The real feasibility of this
50 scenario has, however, yet to be proved, both in terms of real energy harvesting and of
51 compatibility of the machines with a populated area [9-10,13].

52 In particular, Vertical-Axis Wind Turbines (VAWTs), both drag [14-16] and lift-driven [17-
53 20], are gaining popularity in the wind energy scenario, especially in medium and small-size
54 installations, where they can work effectively even in presence of low-speed and unstructured
55 flows with low noise emissions and high reliability. Among others, H-Darrieus rotors are
56 increasingly appreciated in unconventional contexts as they are even assumed to increase their
57 performance in case of an oncoming flow misaligned with respect to the axis of the rotor [17-
58 19]. In order to promote the diffusion of this technology, on one hand, industrial manufacturers
59 are developing new and more appealing design solutions (e.g. [21-25]); on the other hand,
60 efforts are being devoted to reducing the initial cost of the machines (primarily by means of
61 new materials) and to increasing the efficiency, in order to make them competitive with respect
62 to more conventional Horizontal Axis Wind Turbines (HAWTs) [20].

63 Focusing on the commercial aspects, it is also worth pointing out that almost all the industrial
64 rotors are generally designed and optimized for a specific wind speed (i.e. the speed which
65 ensures the highest energy production), but the rated power values, which are often perceived
66 by the final customer as the most valuable indicator of the quality of the product, are declared
67 for their nominal wind velocity, i.e. the highest functioning speed, which provides the
68 maximum power production. Although the importance of accounting for energy instead of
69 power does not come as a surprise for the applied-energy technicians, the implications of this
70 theoretical dichotomy are quite often not completely understood by the final customer of small
71 and medium wind turbines.

72 In detail, the actual operating conditions of a rotor over a year can indeed be very far from the
73 nominal one [9-10,26]. In particular, the available wind energy can be concentrated at the lower
74 wind velocities of the yearly distribution in the installation site, which can be often correctly
75 approximated by a Weibull function [27-30]; in addition, the specific features of the final
76 environment (e.g. local accelerations, effects of obstacles, etc.) are very important in
77 determining the real characteristics of the flow which effectively invests the rotor (e.g. [9-10]).
78 As a result, a turbine optimized only for a singular wind speed could provide poor performance
79 during the largest part of its operating time, with a remarkable reduction of the energy
80 produced and, consequently, of the suitability of the investment [10].

81 Stated the above, a design approach based on the maximization of the annual energy-yield
82 (i.e. the sum of the energy contributions at all the wind speeds experienced over the year) was
83 thought to represent a more valuable solution.

84 **2. Energy-yield-based design strategy**

85 The main goal of this study was to define some effective design guidelines for Darrieus wind
86 turbines which would be able to ensure the maximum energy harvesting in a yearly horizon as
87 a function of the attended wind distribution in the installation site.

88 With this goal in mind, 21600 test cases, i.e. permutations of a specific geometrical
89 configuration (300 cases), an airfoil (4 selections), a wind distribution (6 cases) and a load
90 system (3 cases), were tested and analyzed by means of a specifically developed numerical
91 code based on an advanced BEM method, in order to highlight the configurations which ensure
92 the largest annual energy yield for each wind condition.

93 **2.1 Wind distributions**

94 As a first step of the analysis, six annual wind profiles were hypothesized. As discussed, the
95 most logical representation of the annual wind distribution must be based on the assumption of
96 a Weibull distribution [27-30]. In particular, in the present study a constant shape factor equal

97 to 2.0 (Rayleigh distribution) was considered, whereas the scale factor was modified in each
98 case in order to ensure an average wind speed (\bar{U}) increasing by one from 3 to 8 m/s.

99 The choice of the Rayleigh distribution was based on literature data [9-10], which found that
100 this particular Weibull curve nicely approximates the wind distributions of some medium-low
101 velocity sites in Europe. The presented method, however, is of general validity and can be
102 applied to any Weibull distribution attended in the installation site.

103 In further detail, the wind profiles investigated in this study are shown in Figure 1, where the
104 cut-in and the cut-out limits are also displayed. In particular, it is worth pointing out that a
105 maximum cut-out velocity of 18 m/s was imposed for safety reasons to all the tested rotors
106 [26], based on the industrial experience for these rotors. On the other hand, the cut-in speed
107 was specifically calculated for each rotor on the basis of its behavior at low wind speeds: as
108 shown by Figure 1, a variable cut-in speed between 2 and 3 m/s was measured in the tested
109 rotors. In particular, it is worth pointing out that in the present study the attention was focused
110 only on the Darrieus machines, evaluating their actual self-starting characteristics. Although
111 recent studies (e.g. [31-32]) showed indeed that the self-starting can be enhanced by coupling
112 these rotors with drag-driven devices, the matching of the two turbines was not considered in
113 the scope of the present work and destined to further studies.

114 **2.2 Main design parameters for Darrieus-type turbines**

115 The proper set of rotor configurations to be analyzed was then defined. Due to the large
116 number of variables involved in the aerodynamic design of Darrieus rotors [20,26], some
117 preliminary assumptions were needed to focus the analysis on a significant family of turbines.

118 In particular, the following main choices were made:

- 119 ■ The H-Darrieus configuration with straight blades was selected (see Figure 2). This turbine
120 shape is presently the most exploited and studied solution in Darrieus turbines design, due
121 to higher efficiency and lower manufacturing costs with respect to original troposkien-
122 bladed rotors [20,24,33].

149 would consist in a direct increase of the chord c (Eq. 1). This solution is definitely able to
150 accomplish the goal, but strict limitations to its use must be introduced. In particular, notably
151 longer chords produce both a reduction of the Aspect Ratio of the blade (i.e. the ratio between
152 the blade length and the chord - Eq. 2) and an increase of the solidity of the rotor (Eq. 3)
153 [21,24,26].

154
$$AR_b = \frac{H}{c} \quad (2)$$

155
$$\sigma = \frac{Nc}{D} \quad (3)$$

156 The first effect actually results in a detriment of the blade efficiency [18,21], as the increase
157 of the rotor's height to compensate cannot be always provided as the swept area of the rotor is
158 generally a priori selected (Eq.4 for an H-Darrieus).

159
$$A = H \cdot D \quad (4)$$

160 On the other hand, an increase of the solidity also produces a reduction of the peak efficiency
161 of the rotor [20,21,24], which once more cannot be simply compensated by reducing the
162 diameter because this countermeasure would directly reduce the peripheral speed, thus leading
163 to an undesired reduction of the relative speed W (given by the vector sum of the peripheral
164 speed and the wind speed reduced by the induction factor a - see Eq.5):

165
$$W = \omega R + U(1 - a) \quad (5)$$

166 The second way to control the Reynolds number on the blade is in fact the modification of the
167 relative speed. Having assumed that the wind speed U is fixed, the only way to modify w is
168 related to a variation of the peripheral speed ωR .

169 Analogous to the previous analysis a double choice is given. An increase of the turbine radius
170 would directly improve the Reynolds number: being A fixed, the turbine's height would be
171 reduced (Eq. 4) and then the Aspect Ratio of the blades (Eq.2), leading to less efficient blades.
172 On the other hand, increasing the revolution speed would improve the relative speed, having,

173 however, a notable impact on the incidence angles range and the structural behavior of the
174 rotor.

175 Based on the above, the influence of the selected parameters can be readily highlighted.

176 ▪ **Φ ratio** - The Φ ratio has a double effect in defining the features of the rotor. From an
177 aesthetic point-of-view, it can be considered as a “shape factor” of the turbine, i.e. an
178 indicator of the visual proportions of the virtual cylinder swept during the revolution. On
179 the other hand, for a fixed swept area, low Φ values are typical of a machine in which the
180 optimal flow conditions on the airfoil are obtained thanks to large diameters in order to
181 increase the peripheral speed. In this configuration, the velocity triangles on the airfoils are
182 improved but the blades are generally short, with more relevant losses due to end-effects.
183 Conversely, high Φ values can be related to machines in which the efficiency of the blade
184 (high blade Aspect Ratios - Eq. 2) is preferred.

185 ▪ **ζ ratio** - The c/D ratio is a direct indicator of the solidity (σ) of the rotor (Eq. 3). High
186 values of ζ generally indicate that the chord length is increased to improve the Reynolds
187 number, whereas low ζ values can be related to rotors in which the relative wind speed is
188 increased by means of an increase of the relative wind speed on the airfoil (Eq. 5).

189 ▪ **Swept Area (A)** - As one can argue from the previous discussion, the swept area of the
190 turbine (Eq. 4 - valid for an H-Darrieus rotor) is unfortunately a dimensional parameter
191 which cannot be bypassed in the analysis of small rotors. In particular, larger swept areas
192 ensure less demanding limits of the turbine’s radius, ensuring higher peripheral speed and,
193 therefore, fewer problems in ensuring a good Reynolds number on the blades. Moreover,
194 being the optimal solidity ranges generally constant [20-21], the minimum requested
195 chords are generally smaller, resulting in higher Aspect Ratios and more efficient blades.

196 ▪ **Design variables** - The airfoil type is very important in defining the performance of a
197 Darrieus turbine; as a result, the dimensionless analysis on the best design trends must be
198 individually carried out for each specific airfoil family [20,34-35]. Finally, the struts’

199 shape and dimensions must be carefully taken into account as they can substantially
200 modify the power output of an H-Darrieus rotor (see Refs. [21,24,33,36]) due to the
201 parasitic torque that is produced during the revolution. To this purpose, the impact of the
202 struts was also included in this study by assuming a variation of their dimensions, and even
203 number, as a function of the structural stresses on the blades.

204 **3. Test plan and design parameters**

205 The test plan of the investigated configurations is summarized in Table 1.

206 The limits of the ζ and Φ parameters were defined on the basis of a survey of the technical
207 literature (e.g. [5,20,24]). In particular, the ξ range was limited to 0.200 as higher values would
208 lead to solidities higher than 0.6. Design choices over this limit are in fact considered to be
209 unsuitable for H-Darrieus rotors [20,24], due to the fact that the turbine is deemed to become
210 similar to a solid obstacle for the wind and the interactions between upwind and downwind
211 blades becomes so strong to compromise the aerodynamics of the airfoils. In addition, the
212 theory applied in the simulations could become less predictive in similar test-cases [20].

213 The choice of the aerodynamic airfoils was also based on a literature survey [5,20-21]. In
214 particular, four different airfoils were investigated in this work, in order to highlight the impact
215 of their aerodynamic characteristics on the effective energy harvesting of the turbine. The
216 airfoils were selected among the 4-digit NACA family, which is quite a conventional solution
217 in Darrieus VAWTs [5,20,34-35].

218 In detail, three uncambered airfoils with different thickness/chord ratios (NACA0012,
219 NACA0015, NACA0018) were compared to an asymmetrical and lightly-cambered airfoil
220 (NACA4415). The first group of airfoils is a widely exploited solution in Darrieus turbines, as
221 it ensures a suitable resistance to the stall coupled with good lift outputs at medium-range
222 Reynolds numbers. Moreover, a symmetric airfoil is able to provide the same lift contribution
223 either with positive or negative incidence [20,24]. On the other hand, a cambered profile, like
224 the selected NACA4415, has been suggested in technical literature (e.g. see [5,21]) as an

225 interesting design choice in order to ensure high peak values of the torque in low-velocity
226 cases, although some doubts on their effective application are due to the different behaviour of
227 a non-symmetric airfoil in case of a positive or negative incidence [21].

228 Focusing on the boundary conditions in terms of loads applied to the rotor, three different
229 configurations were analyzed:

230 ▪ **CASE 1 – Aerodynamics only:** in this configuration, the contribution of the resistant
231 torque of the struts was not considered. By doing so, this configuration actually refers to a
232 hypothetical solution of a fully aerodynamic relationship between the geometrical features
233 of the rotor and the power performance. Although not practically applicable, the analysis
234 of these results allows one to define the aerodynamic trends and to directly compare the
235 functioning behavior of machines having different areas. Moreover, by defining the purely
236 aerodynamic requests, one can also directly identify the effects induced by the secondary
237 and parasitic effects due to auxiliary organs (e.g. the struts) and external loads.

238 ▪ **CASE 2 – Centrifugal load:** the contribution of the resistant torque of the struts was again
239 not considered but a limitation on the centrifugal stress acting on the blades was added as a
240 function of the rotational speed of each model.

241 ▪ **CASE 3 – Struts’ parasitic torque:** in this latter configuration, both a limitation on the
242 centrifugal stress on the blades and variable struts dimensions, as a function of the
243 rotational speed of each model, were included. Moreover, the resistant torque of the struts
244 was taken into account.

245 In order to give a correct estimation of the structural loads, in this study a manufacturing
246 technology based on extruded aluminium blades with a hollowed section was considered,
247 utilizing real data on both the maximum centrifugal stress and on the maximum mechanical
248 stress on the struts available from previous design experiences of the authors [33].

249 In further detail, in Case 2 the cut-out speed of the turbine was calculated in each case-study
250 based on the hypothesis that the maximum centrifugal stress at the middle of the blade (where

251 the maximum displacement is located) would not exceed a fixed stress limit of the blade itself
252 (Eq. 6).

$$253 \quad \zeta_b = \frac{F_b}{A_{res_b}} = \frac{m_b \omega^2 R}{A_{res_b}} \leq \zeta_{lim_b} \quad (6)$$

254 where A_{res_b} is a conventional resistance area which takes into account the structure of the
255 stiffeners inside the airfoil and F_b is the centrifugal stress of the blade of mass m_b . In particular,
256 all the airfoils were reproduced with a hollowed section having a constant skin thickness (3
257 mm) and three, equally spaced, rectangular stiffeners perpendicular to the chord of variable
258 thickness. The trailing edge was considered as solid with a filet radius increasing proportionally
259 to the chord of the blade (Figure 3). Based on the characteristics of an aluminium alloy tested
260 by the authors in a previous industrial experience [33,37], a stress limit of 90 N/mm² was here
261 considered.

262 In addition, in Case 3 even the dimensions of the struts (at least two for each blade) are
263 variable from one configuration to another in order to satisfy the stress limit of the blades due
264 to the centrifugal force (Eq. 7 with the same notation of Eq. 6).

$$265 \quad \zeta_{ST} = \frac{F_{ST}}{A_{res_ST}} = \frac{1}{N_{ST}} \frac{m_b \omega^2 R}{A_{res_ST}} \leq \zeta_{lim_ST} \quad (7)$$

266 It is worth pointing out that the load case considered in Eq. 7 takes into account only the
267 tensile stresses generated by the centripetal acceleration of the rotor. In authors' experience
268 (see [33,37]), this load condition is quite realistic for small-size rotors (i.e. with a swept area up
269 to 4.0 m²), whereas bending forces become significant in larger rotors with high Φ ratios. In
270 this work, the bending stresses were neglected but a more accurate description of their
271 influence will be carried out in future works.

272 A correct evaluation of the strut's dimensions is particularly important in small rotors due to
273 the fact that a fast-rotating turbine often needs thick supporting struts to balance the centrifugal

274 stresses [24]. Similar struts, however, are characterized by a notable parasitic torque generation
275 which causes a remarkable detriment of the overall performance of the machine.

276 In particular, in this study a constant shape of the struts was considered. In case of
277 symmetrical airfoils, the same profiles were used. On the other hand, when the NACA4415 is
278 used, the struts are supposed to be realized with the NACA0015 (same t/c ratio but straight
279 camber). By these choices, a constant virtual drag coefficient [24] during the revolution was
280 considered, whereas the dimensions of the struts were varied in Case 3 until the minimum ones
281 which satisfied Eq. 7 were found. In detail, the chord of the struts (and consequently also the
282 thickness, being the t/c ratio fixed) was calculated on the basis of the resistant area defined by
283 Eq.7. When the calculated struts dimensions exceeded the chord of the blade, the struts number
284 was increased by one for each blade and the new dimensions of each element were re-
285 calculated on the basis of the same procedure, in all the investigated configuration, a maximum
286 struts' number of three was constantly observed. Finally, the effects of "bluff-section" struts
287 was investigated, in order to stress more evidently the influence of the parasitic phenomena: the
288 struts were assumed to have a constant virtual drag of 0.3 and a thickness varying with the
289 same procedure described for the airfoil-shaped solutions.

290 **4. Simulations and data reduction**

291 The performance simulations of the machines were carried out with the *VARDAR* code of the
292 Department of Industrial Engineering of the University of Florence. The code makes use of the
293 Blade Element Momentum (BEM) Theory, by which the rotor performance is calculated
294 coupling the momentum equation in the mainstream direction of the wind and a one-
295 dimensional aerodynamic analysis of the interactions between the airfoils in motion and the
296 oncoming flow on the rotor [20,33,38-39] by means of pre-calculated polars. Even if more
297 advanced simulations techniques (including computational fluid dynamics) are today available
298 for the simulation of VAWTs (e.g. [39-41]), BEM approaches are still the most widely
299 exploited tools for the preliminary design of these rotors, as they provide sufficiently reliable

300 results in terms of global performance (whereas a poor description of the instantaneous flow
 301 field around the rotor is achieved) coupled with a notably reduced computational cost.

302 In particular, the VARDAR code has been specifically developed for H-Darrieus wind
 303 turbines using an improved version of a *Double Multiple Streamtubes Approach with Variable*
 304 *Interference Factors* [17,28,42] (Figure 4a). In this approach, the elementary torque for each
 305 azimuthal position is therefore given by Eq. 8:

$$306 \quad T_{blade}(\vartheta) = F_t \cdot R = \frac{1}{2} \rho c W_{\vartheta}^2 C_{t(\vartheta)} R H \quad (8)$$

307 where C_t and W represent the tangential coefficient of the airfoil in the reference system of the
 308 rotating blade (Figure 4b) and the relative velocity of the flow experienced by the airfoil itself
 309 in the upwind or downwind half, respectively, expressed by Eqs. 9,10 and 11:

$$310 \quad C_t = C_L \cdot \sin \alpha - C_D \cdot \cos \alpha \quad (9)$$

$$311 \quad W_{up} = \sqrt{[(1-a) \cdot U_{\infty} \cdot \sin(\vartheta - \beta)]^2 + [(1-a) \cdot U_{\infty} \cos(\vartheta - \beta) + \omega R]^2} \quad (10)$$

$$312 \quad W_{down} = \sqrt{[(1-a_2) \cdot U_{eq} \cdot \sin(\vartheta - \beta)]^2 + [(1-a_2) \cdot U_{eq} \cos(\vartheta - \beta) + \omega R]^2} \quad (11)$$

313 As for the more general Eq. 5, the relative speed is given by the sum of peripheral speed and
 314 wind speed, properly reduced by the induction factor (either upwind or downwind). The value
 315 U_{eq} in Eq. 25 indeed represents the wind equilibrium velocity between actuator disks (see
 316 Figure 4).

317 The Glauert's correction for the BEM theory has been taken into account with the most recent
 318 improvements, together with the corrections due to blades finite Aspect Ratio, using the
 319 Lanchester-Prandtl model. This aspect is of particular relevance in the present analysis, as it
 320 allows the designer to account for the increasing tip-losses connected to blades with small
 321 height to chord ratios.

322 In order to increase the accuracy of the aerodynamic estimations, a specific sub model to
 323 account for the dynamic stall has been provided, following the Paraschivoiu's adaptation to the

324 DMS approach described in; at the same time, the stream tube expansion along the flow path
 325 was considered. For additional details on the code please refer to Refs. [23,26,33,37,42-43].

326 The prediction capabilities of the VARDAR code have been validated during a several-years'
 327 experience in the design of three real H-Darrieus rotors, having swept areas of 1, 2.5 and 5 m²,
 328 respectively, and two or three blades, either straight or helix-shaped. The 1:1 models of all the
 329 rotors (two made of reinforce plastic and one of painted aluminium alloy) were tested in
 330 different wind tunnels (both with closed and open-jet). In all cases, the code was able to
 331 correctly predict both the power curves at different wind speeds and the starting ramps of rotor
 332 and is then considered fully predictive for the turbine typology investigated in this study. For
 333 further details on the code validation please refer to Refs. [23,33,37,42].

334 In the present analysis, the code provided the power coefficient of each configuration at all
 335 the wind speeds between the cut-in and the cut-out. The characteristic power coefficient of the
 336 machines at each wind velocity was conservatively evaluated in correspondence with the
 337 calculated performance 0.2 points of TSR after the peak of the operating curve. A similar
 338 precaution is often applied in order to define a load curve aimed at preventing the turbine from
 339 operating in the unstable part of the functioning curve [11,24]. Moreover, it is worth noticing
 340 that the cut-in speed in each case was set to the wind speed for which a positive power
 341 coefficient is obtained. This is, in fact, a precautionary assumption, because the self-starting of
 342 an H-Darrieus rotor in real wind is often ensured for several starting positions even if the
 343 overall power coefficient over the revolution is negative [42,45].

344 In further detail, for each configuration in terms of swept area (i.e. the discrete variable of the
 345 problem) specific performance maps were created [26] corresponding to a given wind
 346 distribution. Each map (e.g. see Figure 5) contains the overall efficiency of energy conversion
 347 (η_{en}) of the specific rotor, defined as in Eq. 12 and 13.

$$348 \quad \eta_{en} = \frac{\sum_{u=cut-in}^{cut-out} c_p(u) \cdot u^3 \cdot T(u)}{\sum_{u=cut-in}^{cut-out} u^3 \cdot T(u)} \quad (12)$$

349
$$T(u) = f(u) \cdot 8760 \quad (13)$$

350 Upon examination of the equations, it is worth pointing out that the energy conversion
351 efficiency was defined as the annual energy yield of the turbine over the year (i.e. the real
352 extracted power at each wind speed multiplied by the time fraction, in hours, during which that
353 wind blows $T(u)$) on the theoretical energy contained in the wind itself.

354 Based on its definition, this indicator differs from the classical power coefficient and allows
355 one to simultaneously take into account both the efficiency of the turbine at all the wind speeds
356 expected over the year and the effects related to the starting and resistance capabilities of the
357 rotor (due to the variable cut-in and cut-out velocities considered).

358 Finally, within each map, a numerical identification of the maximum was performed, with the
359 constraints of neglecting design solutions which imply Blade's Aspect Ratios higher than 35: in
360 case of excessive ratios between the height and the chord, the bending resistance of such a
361 slender blade would be indeed very poor, making the selected solution practically unfeasible.

362 This procedure would finally lead to the definition of the geometrical features of the rotor
363 ensuring the largest energy harvesting over a year for the attended load case, average wind
364 speed in the site and imposed swept area of the rotor.

365 The whole data reduction procedure is summarized in Figure 6, while a complete overview on
366 the results in terms of best design solutions can be find in the Appendix Section.

367 **5. Results**

368 **5.1 Energy Efficiency maps interpretation**

369 A typical Energy Efficiency map has been presented in Figure 5 (e.g. for a swept area of 4.0
370 m^2 , NACA0018 airfoil, $\bar{U}=5$ m/s in Case 2). A linear interpolation was performed between the
371 calculated points (see Table 1) in order to more precisely outline the contours.

372 It is readily noticeable that an optimum-design zone (white-colored in the figure) can be
373 typically distinguished in the bottom side. This zone represents the combination of the Φ and ζ

374 parameters which ensures the best compromise in terms of functioning Reynolds numbers on
375 the airfoil (high peripheral speeds and chords) and efficiency of the blades (high Aspect
376 Ratios). Moreover, one can also notice that the efficiency is almost zero in the left side of the
377 map, where the very small chords remarkably reduce the lift generation, and becomes lower
378 also in the right-bottom corner of the map, where the turbine heights tend to zero.

379 As discussed, within each map a numerical identification of the maximum was performed in
380 order to define the geometrical features of the rotor ensuring the largest energy harvesting over
381 a year under the present design constraints.

382 **5.2 Case 1 - Aerodynamics**

383 From a general point of view, it is worth remembering that Case 1 configuration actually
384 refers to a hypothetical solution of a fully aerodynamic relationship between the geometrical
385 features of the rotor and the power performance. By doing so, the influence of the main
386 aerodynamic design parameters can be readily argued and the functioning behaviors of
387 machines having different areas can be directly compared.

388 The main outcome of the analysis of Case 1 is that an opposite behavior was found between
389 cambered and uncambered airfoils in this configuration.

390 As an example of uncambered airfoils, Figure 7 reports the variation trends which describe
391 the dependence of the optimal values of the most relevant design parameters from the average
392 wind speed for the NACA0015 airfoil.

393 Upon examination of Figure 7, some relevant markups can be promptly made. In particular:

- 394 ■ The dimensionless parameters present the same trends even when different swept areas are
395 considered, although numerical values differ from one configuration to another,
396 confirming that scale effects must be taken into account.
- 397 ■ When the average wind speed in the site increases, the best solidity decreases constantly
398 and the Aspect Ratio rises significantly, whereas the Shape Factor Φ increases for

399 medium-low average wind speeds and then becomes stable. As a general remark, however,
400 the turbine tends to become slenderer by increasing the average wind speed.

401 ■ Focusing on the dimensional parameters, the aforementioned trend is basically obtained
402 throughout a constant decrease of the blades' chord with the average wind speed increase
403 (with a steeper trend for medium-low \bar{U} and a flatter trend with an increased \bar{U}). The
404 turbine diameter and height have instead an opposite trend, with a decrease and an increase
405 in the first part, respectively, followed by a constant trend in the second part.

406 The main aerodynamic implication of these results is that, when the average wind velocity
407 experienced by the turbine is low (left side of the plots), the best design is that ensuring the
408 highest local Reynolds numbers on the blade by means of the geometrical proportions. As a
409 consequence, the chord values are maximized (see Eq. 1) at low wind speeds and then the
410 solidity values are high (Eq. 3).

411 By increasing the average wind speed, the velocity triangles on the airfoils are altered thanks
412 to the increased relative velocities experienced by the blades: the chords can be therefore
413 reduced without decreasing the functioning Reynolds numbers. For high mean wind velocities,
414 however, the chord length stops decreasing and more efficient blades (i.e. higher Aspect Ratios,
415 $AR=H/c$ [20-21,24]) are obtained by means of an increase of the turbine height (black curves in
416 the graphs on the left). The optimal solidity constantly decreases with \bar{U} .

417 Moreover, a well-defined dependence on the t/c ratio of the airfoil was observed. For
418 example, in Figures 7 and 8 the optimal trends of the solidity and the blade's Aspect Ratio for
419 the three uncambered airfoils are reported.

420 In detail, by decreasing the t/c ratio of the selected airfoil (Figure 8), i.e. from NACA0018 to
421 NACA0015 and NACA0012, the optimal solidity of the turbine is constantly reduced. This
422 phenomenon can be related to a decrease of the requested chord. This solution is indeed
423 allowed by an increase of the target peripheral speed of the rotor which, on one hand, ensure a
424 suitable Reynolds number on the airfoil (Eq.1) and, on the other hand, decreases the incidence

425 angles range: thinner airfoils (e.g. the NACA0012), although more efficient for high relative
426 speeds, have indeed a lower stall angle and are generally more sensitive to incidence angle
427 variations. Contemporarily (Figure 9), the same reasons induce an opposite behavior of the
428 blade's Aspect Ratio (AR_b), which is constantly higher in case of thinner airfoils (the shorter
429 chords are combined with an almost equal trend of optimal heights).

430 The optimal design trends in case of the cambered NACA4415 airfoil are notably different. In
431 particular, whenever this typology of profile is applied, the scale effects due to the swept area
432 become negligible, as the high C_L/C_D ratio of this airfoil [44] makes the dependence of the
433 aerodynamic performance from the chord very low. The Aspect Ratio can then rise
434 significantly to pursue the higher blade's efficiency. The optimal design proportions in Case 1
435 for the NACA4415 airfoil are reported in Figure 10. In this configuration, the optimal solidity
436 is low (see Eq. 3) and the AR_b very high mainly due to the very short chords.

437 **5.3 Case 2 - Limited centrifugal load**

438 The results obtained from the examination of Case 1 are very useful to comprehend the
439 aerodynamic trends connected to a variation of the wind velocities experienced by the turbine;
440 structural constraints like the centrifugal load have, however, relevant impact on the best design
441 compromise of a machine [24,26].

442 To this purpose, next figures report some results of the investigation on the study-cases in
443 Case 2, in which a $\zeta_{lim,b}$ (Eq. 6) of 90 N/mm^2 was considered [26,33]; for a wider overview of
444 the results, please see Appendix B.

445 First, it was noticed that, when the average wind velocities are low (i.e. $3\div 4 \text{ m/s}$), the
446 structural constraints actually do not affect the definition of the best design parameters; the
447 operating rotational speeds at these velocities are low and the resulting centrifugal loads do not
448 exceed the structural limits. In case of the NACA4415, the best design is once again imposed
449 due to limitation on the blade's Aspect Ratio.

450 Once again, the two types of airfoils work differently. If the uncambered profiles are selected
451 and the medium-high wind speeds become more frequent, the reduction of the solidity with the
452 average wind speed noticed in Case 1 ceases (an almost constant value is reached – e.g. see
453 Figure 11), mainly due to the stop in the decrease of the optimal chord (Figure 12).

454 This trend can be explained by considering that, when the wind velocities are high, the most
455 suitable compromise in terms of energy-yield capabilities comes from a reduction of the peak
456 efficiency of the turbine (higher solidity) which, however, implies a reduction of the operating
457 rotational regime [24,26]. This reduction makes the centrifugal loads decrease and allows the
458 turbine to extract energy from the wind with all the considered wind velocities.

459 In particular, after examining the Energy Efficiency maps (e.g. for the NACA0018, swept
460 area $A=4 \text{ m}^2$ in Figure 13), it is readily noticeable that, for low average wind speeds, the best
461 efficiency zone first migrates towards lower solidities and higher Φ ratios. When the high wind
462 speeds become more frequent, however, a new zone of best efficiency arises at higher ζ and Φ
463 ratios.

464 On the other hand, in case the NACA4415 is adopted, the optimal design solution highlighted
465 in Case 1 (small chords, very high AR_b and high revolution speeds) is no longer feasible due to
466 the limitation to the centrifugal load.

467 As a result, the best solidity value is slightly increased for medium-high average wind speeds
468 (Figure 14); contemporarily, the chords and diameters remarkably increase in order to achieve
469 a drastic reduction of the revolution speed (Figure 15). One should indeed remember that
470 longer chords ensure more favorable Reynolds numbers on the airfoil without increasing the
471 relative speed (see Eq. 3), whereas higher diameters act oppositely by improving the relative
472 speed (Eq. 4) or, conversely, ensure the same relative speed with lower revolution speeds.

473 Finally, it is also worth noticing that this increase of the diameter for high average wind speeds
474 is avoided only for high swept areas (i.e. $A=9.0 \text{ m}^2$), where the limit on the centrifugal load is

475 mitigated by the large diameters. In these conditions, the AR_b can be also slightly increased,
476 with a partial recovery of the blades' efficiency (see Appendix B).

477 **5.4 Case 3 - Centrifugal load and struts' parasitic torque**

478 Focusing now on a real-type machine, a further constraint must be included in the
479 identification of the best design trends: the parasitic torque of the struts is, in fact, a key
480 element in defining both the peak efficiency of the machine and its functioning behaviour at
481 different wind speeds. Due to the relevance of this load case, the complete comparison of the
482 optimal design configurations was reported in Appendix D.

483 The calculations showed that the general effect of the parasitic torque is to slightly flatten the
484 trends of the design parameters as a function of the average wind speed. The best design
485 solutions tend in fact to collapse in the configurations that minimize the contribution of the
486 parasitic components [26]. The general tendencies described in Section 4.3 are, however, still
487 of validity and will not be all again discussed. In particular, the efficiency maps shape
488 discussed in Figure 13 was confirmed also under this load case, with the only discussed
489 restriction of the high-efficiency zone. Some interesting remarks can however be made.

490 First, Figure 16 reports the comparison between the optimal solidity trends in Case 2 and 3 for
491 NACA0012 and NACA0018 airfoils (swept area of 1.0 m^2), as a function of the average wind
492 speed. As one may notice, no great difference stands between the two cases when the average
493 wind speed in the site is sufficiently high (i.e. higher than 5 m/s). Conversely, in case of low
494 average wind speeds, the optimal solidity in Case 3 is higher than that obtained in case the
495 parasitic torque is neglected.

496 In order to give a correct interpretation of the results, it is worth remembering that the
497 parasitic torque generated by the rotating structures which do not contribute to the torque
498 generation (e.g. struts, tie-rods, etc.), has a quadratic dependence on the rotational speed of the
499 rotor (directly affecting the tangential velocity) and a lighter and more complex dependence on
500 the wind velocity (see Refs. [33,36]).

501 Based on these considerations, one can understand that, when the wind speeds are low, the
502 impact of the parasitic torque on the effective energy-extraction capability of the rotor is more
503 relevant: as a consequence, the optimal design tends to increase the solidity, in order to achieve
504 a reduction of the revolution regime [24].

505 Focusing on the cambered airfoil, the situation is again quite different (see Figure 17). With
506 this airfoil selection, which is thought to provide a good torque production even in low winds,
507 the best design solution is almost unaltered within $\bar{U}=5$ m/s with respect to Case 2.

508 When the high wind speeds in the site become more frequent, however, the “low solidity”
509 solutions, which are associated with very high revolution speeds, are not suitable anymore, as
510 the parasitic torque has become too high. The optimal solutions hence tend to higher solidities
511 (i.e. slower revolution speeds), very similar to those identified for the uncambered airfoils.

512 Finally, in order to further stress the importance of the parasite torque of the struts, in Figure
513 18 a comparison between the optimal solidity for a turbine with the NACA0012 airfoil and a
514 swept area of 1 m^2 is reported as a function of the strut’s shape. In detail, when the drag of the
515 struts increases, the solidity tends to notably increase, in the attempt of reducing the revolution
516 speed of the rotor. In the selected case, the more energy-efficient solution would be very solid
517 (even up to the limit of $\sigma = 0.6$), which is, however, a practically unfeasible solution. In a
518 similar case, a compromise must be pursued in practically designing the rotor, including a
519 reduction of the effective energy-yield capabilities.

520 At the end of this study, one could then conclude that, from an energy viewpoint, future
521 design of medium and small-size Darrieus rotors should be based on the maximization of the
522 energy yield on the basis of the characteristics of the potential installation site. In particular, for
523 given rotor’s dimensions, a differently shaped turbine would be about to be preferred as a
524 function of the average wind speed of the installation. For example, in Figure 19 the optimal
525 design choices for a turbine having a swept area of 4 m^2 and equipped with NACA0018 airfoils
526 are presented as a function of the average wind speed in the site. In particular, the

527 aforementioned trends in terms of increase of the H/D ratio and decrease of the chord length
528 are clearly distinguishable.

529 For the same family of turbines (presented trends are consistent with all the analyses
530 presented in this study), the annual energy yield of the optimized rotors is presented in Figure
531 20 as a function of the average wind speed in the site. In order to provide a sensitivity analysis
532 on the benefits of the proposed approach, in the same figure the energy yield increase with
533 respect to two others design choices is presented. In further details, Study Turbine A represents
534 a hypothetical turbine designed to have the maximum efficiency at 6 m/s, which could be, for
535 example, the average speed in the site [23]. Study Turbine B instead represents the turbine
536 optimized by means of the maximum-energy-yield criterion at $\bar{U}=6$ m/s.

537 Some very interesting remarks can be done. First, it is worth noticing that a design approach
538 based on the maximum annual energy yield actually provides an increase of performance in all
539 cases. In particular, focusing on the 6 m/s bar, one can notice that benefits can be achieved also
540 in comparison to a design criterion based on the same average speed of the site.

541 Moreover, the proposed criterion is able to provide notable energy increase (up to 10% in the
542 present case) when the wind speeds in the site are low, confirming the prospects of specific
543 future design choices for these conditions.

544 **6. Conclusions**

545 In this study, a numerical analysis has been carried out to define some design guidelines for
546 Darrieus wind turbines aimed at optimizing the annual energy yield of each machine in the
547 installation site. The main outcomes of the analysis can be summarized as follows.

548 Focusing on the only aerodynamic requirements, an opposite behavior was found between
549 cambered and symmetric, uncambered airfoils. For uncambered profiles, when the average
550 wind speed in the site increases, the best solidity decreases constantly, the Aspect Ratio rises
551 significantly, whereas the Shape Factor Φ increases for medium-low average wind speeds and
552 then becomes stable. This trend is mainly due to the fact that, by increasing the wind speed, the

553 relative velocity is increased, and the Reynolds number is improved. The chords can be then
554 reduced, with notable benefits in terms of blade's efficiency. A well-defined dependence on the
555 t/c ratio was also observed: by decreasing the t/c ratio, the optimal solidity is constantly lower
556 whereas higher Aspect Ratios are preferable. When a cambered airfoil is instead selected, the
557 scale effects due to the swept area becomes negligible, as the high C_L/C_D ratio of this airfoil
558 makes the dependence of the aerodynamic performance from the chord very low, hence
559 allowing the Aspect Ratio to rise significantly to pursue the higher blade's efficiency. With this
560 selection, the optimal solidity is consequently also very low.

561 On the other hand, when structural constraints and notable parasitic contributions are
562 introduced, the best configurations when the average wind velocities are low are similar to that
563 coming from the aerodynamic analysis, although the optimal design generally tends to increase
564 the solidity, in order to ensure a better functioning conditions to the airfoils (higher Reynolds
565 numbers, increased torque) and contemporarily achieve a reduction of the revolution regime,
566 which contains the parasitic torque. On the other hand, when the medium-high wind speeds
567 become more frequent, the most suitable compromise in terms of energy-yield capabilities
568 generally comes from a reduction of the peak efficiency of the turbine which, however, ensures
569 a good energy extraction is a wider range of functioning conditions. In case of uncambered
570 airfoils, in particular, this goal is obtained with a general increase of the optimal solidity, which
571 makes the revolution speed decrease and allows the turbine to extract energy from the wind
572 with all the considered wind velocities. As a general remark, however, by increasing the
573 parasitic contributions, the transition of the best design compromise to higher solidity solutions
574 is anticipated, due to the stronger dependence of the performance on the rotational speed.

575 At the end of this work, it has to be noticed that the present analysis was carried out under
576 specific assumptions in terms of dimensions, airfoil types, load system and struts' shape; on
577 these bases, the reader has to consider that different performance maps could come from a new
578 set of theoretical assumptions, although some general trends outlined in the work (e.g. the

579 influence of the turbine proportions on the Reynolds numbers and the rotational speed) are of
580 general validity.

581 The proposed design criterion, however, besides being theoretically more rigorous from a
582 truly energetic point-of-view than a conventional one based on a single reference wind speed,
583 has shown interesting prospects in terms of energy production improving. In particular,
584 different models could be designed for specific wind distributions in order to optimize the
585 energy yield also at low wind speeds, which are very frequent in several countries and in
586 unconventional installation sites, e.g. the urban environment.

587 **Nomenclature**

588	A	Swept Area	$[\text{m}^2]$
589	a	Induction Factor	
590	AR	Aspect Ratio	
591	c	Blade Chord	$[\text{m}]$
592	C_D	Drag Coefficient	
593	C_L	Lift Coefficient	
594	C_t	Tangential Force Coefficient	
595	c_P	Power Coefficient	
596	D	Turbine Diameter	$[\text{m}]$
597	F_n	Normal Force on the Blade	$[\text{N}]$
598	F_{ST}	Force due to Centrifugal Loads	$[\text{N}]$
599	F_t	Tangential Force on the Blade	$[\text{N}]$
600	f	Frequency	
601	H	Turbine Height	$[\text{m}]$
602	m	Mass	$[\text{kg}]$
603	N	Blades/Struts Number	
604	P	Power	$[\text{W}]$

605	R	Turbine Radius	[m]
606	Re_c	Chord-based Reynolds Number	
607	T	Annual Time of each Wind Class	[h]
608	t	Airfoil Thickness	[m]
609	TSR	Tip-Speed Ratio	
610	u	Wind Class	[m/s]
611	U_∞	Absolute Wind Speed	[m/s]
612	\bar{U}	Average Wind Speed	[m/s]
613	W	Relative Wind Speed	[m/s]
614			
615	<u>Superscripts</u>		
616	*	Per Unit Area	
617	\rightarrow	Vectorial Quantity	
618			
619	<u>Subscripts</u>		
620	air	Air	
621	b	Blade	
622	en	Energy	
623	eq	Equilibrium (between upwind and downwind)	
624	res	Resistant Component	
625	ST	Struts	
626			
627	<u>Greek letters</u>		
628	Φ	Turbine Shape Factor	
629	α	Incidence Angle on the Airfoils	[deg]
630	β	Pitch Angle	[deg]
631	η_{en}	Energy-conversion Efficiency	

632	ν	Kinematic Viscosity	$[\text{m}^2/\text{s}]$
633	ζ	Chord/Diameter Ratio	
634	ρ	Air Density	$[\text{kg}/\text{m}^3]$
635	σ	Solidity	
636	ζ	Structural Stress	$[\text{N}/\text{m}^2]$
637	ω	Rotational Speed	$[\text{rad}/\text{s}]$

638 **References**

- 639 [1] Global Wind Report. Global Wind Energy Council; 2011.
- 640 [2] Global Wind Energy Outlook. GWEC, Brussels (Belgium); 2011.
- 641 [3] Oceans of Opportunity. EWEA, Brussels (Belgium); 2009.
- 642 [4] Junginger M, Faaij A, Turkenburg WC. Cost Reduction Prospects for Offshore Wind
643 Farms. *Wind Engineering* 2004;28(1):97–118.
- 644 [5] Kirke BK, Evaluation of self-starting vertical axis wind turbines for standalone
645 applications. Ph.D. thesis, Griffith University, Gold Coast (Australia); 1998.
- 646 [6] Small Wind Turbine Global Market Study. AWEA, Whashington DC (USA); 2008.
- 647 [7] Mertens S. *Wind Energy in the Built Environment*. Brentwood (UK): Multi-Science; 2006.
- 648 [8] Dayan E. Wind energy in buildings: Power generation from wind in the urban environment
649 - where it is needed most. *Refocus* 2006;72(2):33-38.
- 650 [9] Beller C. *Urban Wind Energy - State of the Art 2009*, Risø Laboratory - DTU, Roskilde
651 (Denmark), Tech. rep. Risø-R-1668(EN); 2009.
- 652 [10] Balduzzi F, Bianchini A, Ferrari L. Microeolic turbines in the built environment: influence
653 of the installation site on the potential energy yield. *Renewable Energy* 2012;45:163-174.
- 654 [11] Balduzzi F, Bianchini A, Carnevale EA, Ferrari L, Magnani S. Feasibility analysis of a
655 Darrieus vertical-axis wind turbine installation in the rooftop of a building. *Applied Energy*
656 2012;97:921–929.

- 657 [12] Syngellakis K. Urban wind turbines: Development of the UK market. Proc. of the
658 European Wind Energy Conference 2006, February 27-March 2, Athens (Greece); 2006.
- 659 [13] Banks D, Cochran B, Denoon R., Wood G. Harvesting Wind Power from Tall Buildings.
660 Proc. of the CTBUH 8th World Congress, Dubai (UAE), 2008 In: Chicago: Council on Tall
661 Buildings and Urban Habitat; 2008, pp. 320-327.
- 662 [14] Sarma NK, Biswas A, Misra RD. Experimental and computational evaluation of Savonius
663 hydrokinetic turbine for low velocity condition with comparison to Savonius wind turbine at
664 the same input power. Energy Conversion and Management 2014;83:88-98.
- 665 [15] Roy S, Saha UK. Review of experimental investigations into the design, performance and
666 optimization of the Savonius rotor. Proc. of the Institution of Mechanical Engineers, Part A:
667 Journal of Power and Energy 2013;227(4):528-542.
- 668 [16] Gupta R, Biswas A, Sharma KK, Comparative study of a three-bucket Savonius rotor with
669 a combined three-bucket Savonius-three-bladed Darrieus rotor. Renewable Energy 2008;33(9):
670 1974-1981.
- 671 [17] Mertens S, van Kuik G, van Bussel G. Performance of an H-Darrieus in the Skewed Flow
672 on a Roof. Journal of Solar Energy Engineering 2003;125:433-440.
- 673 [18] Simão Ferreira CJ, van Bussel G, van Kuik G. An analytical method to predict the
674 variation in performance of a H-Darrieus in skewed flow and its experimental validation. Proc.
675 of the European Wind Energy Conference, February 27-March 2, 2006, Athens (Greece); 2006.
- 676 [19] Bianchini A, Ferrara G, Ferrari L, Magnani S, An improved model for the performance
677 estimation of an H-Darrieus wind turbine in skewed flow. Wind Engineering 2012;36(6):667-
678 686.
- 679 [20] Paraschivoiu I, Wind Turbine Design with Emphasis on Darrieus Concept. Polytechnic
680 International Press, Canada; 2002.

681 [21] Bianchini A, Ferrari L, Magnani S. Analysis of the Influence of Blade Design on the
682 Performance of an H-Darrieus Wind Turbine. Proc. ASME-ATI-UIT 2010 Conference on
683 Thermal and Environmental Issues in Energy Systems, Sorrento (Italy) May 16-18; 2010.

684 [22] Sharpe T, Proven G. Crossflex: Concept and early development of a true building
685 integrated wind turbine. *Energy and Buildings* 2010;42:2365-2375.

686 [23] Bianchini A, Ferrari L, Schneider A. First steps in the design and optimization of Darrieus
687 VAWTs for microeolic applications. Proc. World Renewable Energy Congress (WREC) X,
688 Glasgow (Scotland), July 19-25; 2008.

689 [24] Ferrari L, Bianchini A. Critical aspects in the design of a small-size Darrieus wind turbine.
690 Proc. World Renewable Energy Congress (WREC) XI, Abu Dhabi (UAE) September 25-30;
691 2010.

692 [25] Aslam Bhutta MM, Hayat N, Farooq AU, Ali Z, Jamil ShR, Hussain Z, Vertical axis wind
693 turbine – A review of various configurations and design techniques. *Renewable and*
694 *Sustainable Energy Reviews* 2012;16(4):1926-1939.

695 [26] Bianchini A, Ferrari L, Magnani S. Energy-yield-based optimization of an H-Darrieus
696 wind turbine. Proceedings of the ASME Turbo Expo 2012, Copenhagen (Denmark), June 11-
697 15; 2012.

698 [27] Manwell JF, McGowan JG, Rogers AL. *Wind Energy Explained*, 2nd edition, Wiley,
699 U.K.; 2009.

700 [28] Justus CG, Hargraves WR, Mikhail A, Graber D. Methods for estimating wind speed
701 frequency distributions. *Journal of Applied Meteorology* 1978;17(3):350-353.

702 [29] Akdağ SA, Dinler A. A new method to estimate Weibull parameters for wind energy
703 applications. *Energy Conversion and Management* 2009;50(7):1761-1766.

704 [30] Freitas de Andrade C, Maia Neto HF, Costa Rocha PA, Vieira da Silva ME. An efficiency
705 comparison of numerical methods for determining Weibull parameters for wind energy

706 applications: A new approach applied to the northeast region of Brazil. *Energy Conversion and*
707 *Management* 2014;86(10):801-808.

708 [31] Bhuyan S, Biswas A. Investigation on self-starting and performance characteristics of
709 simple h and hybrid H-Savonius vertical axis wind rotors. *Energy Conversion and Management*
710 2014;87:859-867.

711 [32] Gupta R, Das R, Sharma KK. Experimental study of a Savonius-Darrieus wind machine.
712 In *Proceedings of the International Conference on Renewable Energy for Developing*
713 *Countries*, University of Columbia, Washington DC, 2006.

714 [33] Bianchini A. Performance Analysis and Optimization of a Darrieus VAWT. PhD Thesis,
715 School of Energy Engineering and Innovative Industrial Technologies, University of Florence
716 (Italy); 2011.

717 [34] Islam M, Ting D, Fartaj A, Desirable Airfoil Features for Smaller-Capacity Straight-
718 Bladed VAWT. *Wind Engineering* 2007;31(3):165–196.

719 [35] Klimas PC. Tailored Airfoils for Vertical Axis Wind Turbines. Sandia National
720 Laboratories, Albuquerque, N.M., SAND 84-1062; 1984.

721 [36] Paraschivoiu I, Delclaux F. Double Multiple Streamtube Model with Recent
722 Improvements. *Journal of Energy* 1983;7(3):250-255.

723 [37] Balduzzi F, Bianchini A, Maleci R, Ferrara G, Ferrari L. Blade design criteria to
724 compensate the flow curvature effects in H-Darrieus wind turbines. *Journal of Turbomachinery*
725 2015;137(1):1-10.

726 [38] Camporeale SM, Magi V. Streamtube model for analysis of vertical axis variable pitch
727 turbine for marine currents energy conversion. *Energy conversion and Management*
728 2000;41(16):1811-1827

729 [39] Islam M, Ting D SK, Fartaj A. Aerodynamic models for Darrieus-type straight-bladed
730 vertical axis wind turbines. *Renewable and Sustainable Energy Reviews* 2008;12:1087-1109.

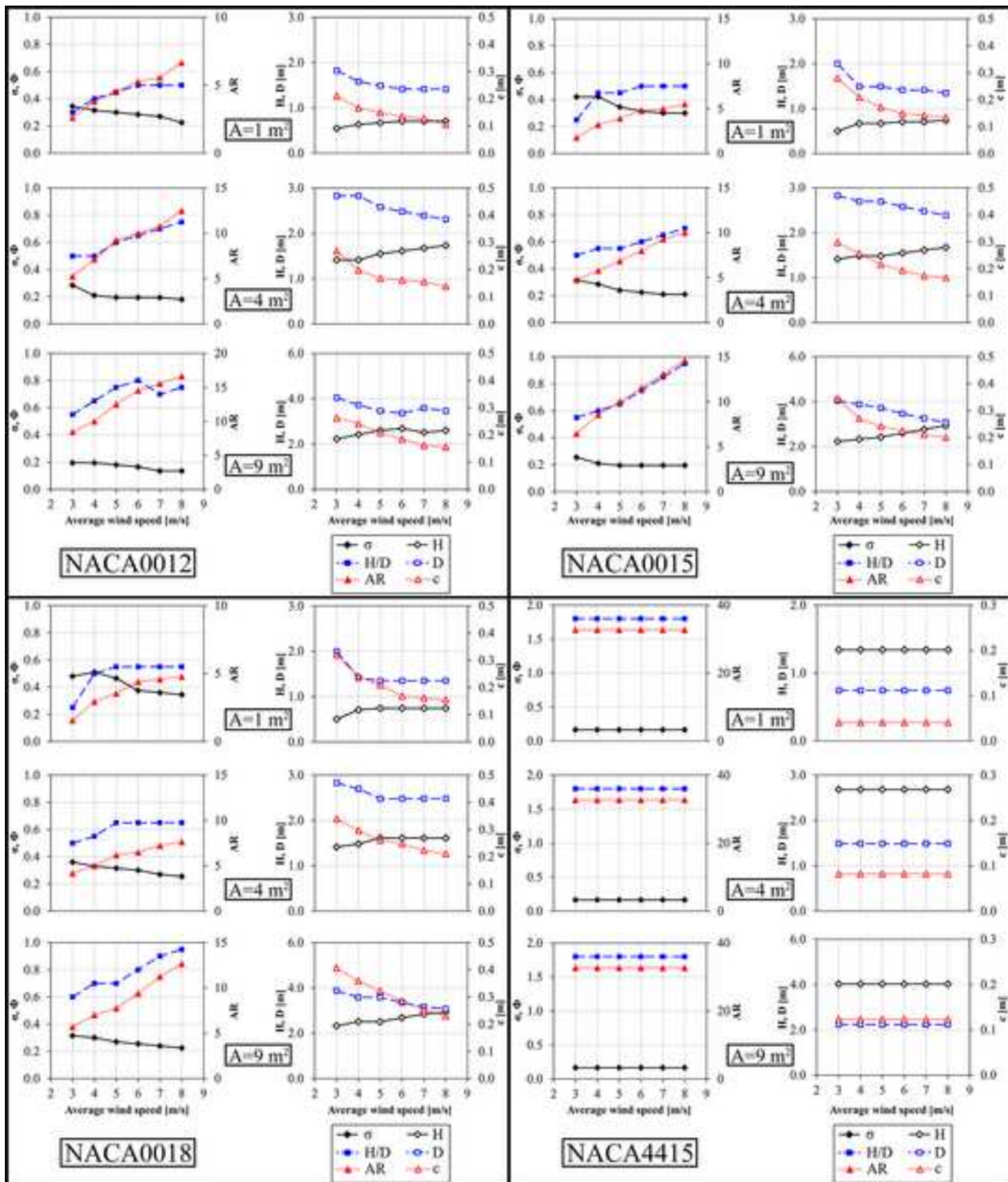
- 731 [40] Wang LB, Zhang L, Zeng ND. A potential flow 2-D vortex panel model: Applications to
732 vertical axis straight blade tidal turbine. *Energy Conversion and Management* 2007;4(2):454-
733 461.
- 734 [41] Simão Ferreira CJ. The near wake of the VAWT: 2D and 3D views of the VAWT
735 aerodynamics. PhD Thesis, Technische Universiteit Delft, The Netherlands, 2009.
- 736 [42] Bianchini A, Ferrari L, Magnani S. Start-up behavior of a three-bladed H-Darrieus
737 VAWT: experimental and numerical analysis. Proc. of the ASME Turbo Expo 2011,
738 Vancouver (Canada), June 6-10; 2011.
- 739 [43] Bianchini A, Ferrari L, Carnevale E.A.. A model to account for the Virtual Camber Effect
740 in the Performance Prediction of an H-Darrieus VAWT Using the Momentum Models. *Wind*
741 *Engineering* 2011;35(4):465-482.
- 742 [44] Ostowari C, Naik D. Post stall studies of untwisted varying aspect ratio blades with an
743 NACA 4415 airfoil section - Part I. *Wind Engineering* 1984;8(3):176-194.
- 744 [45] Dominy R, Lunt P, Bickerdyke A, Dominy J. Self-starting capability of a Darrieus turbine.
745 Proc. IMechE 221 Part A: Journal of Power and Energy 2007:111-120.

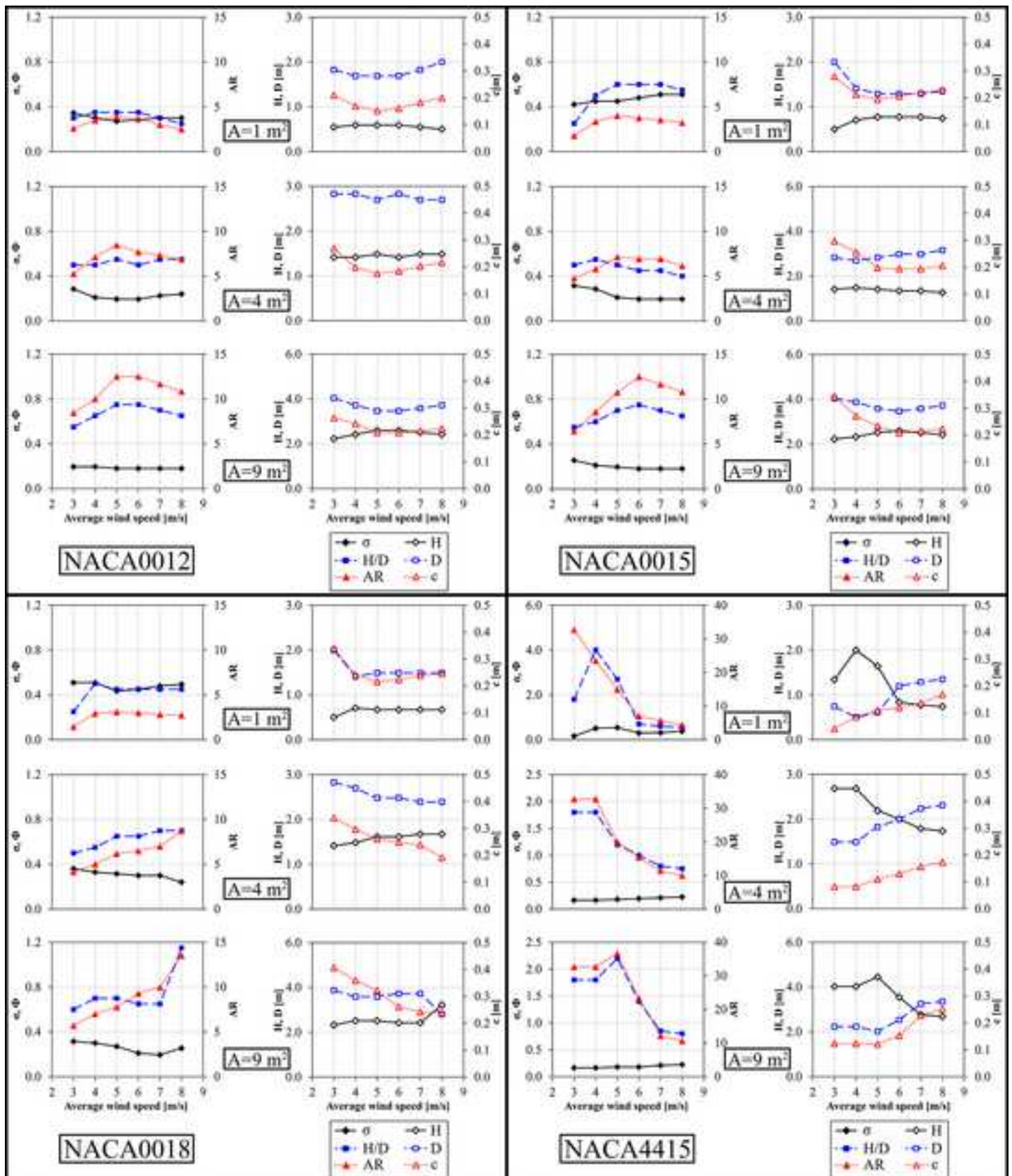
Table(s)

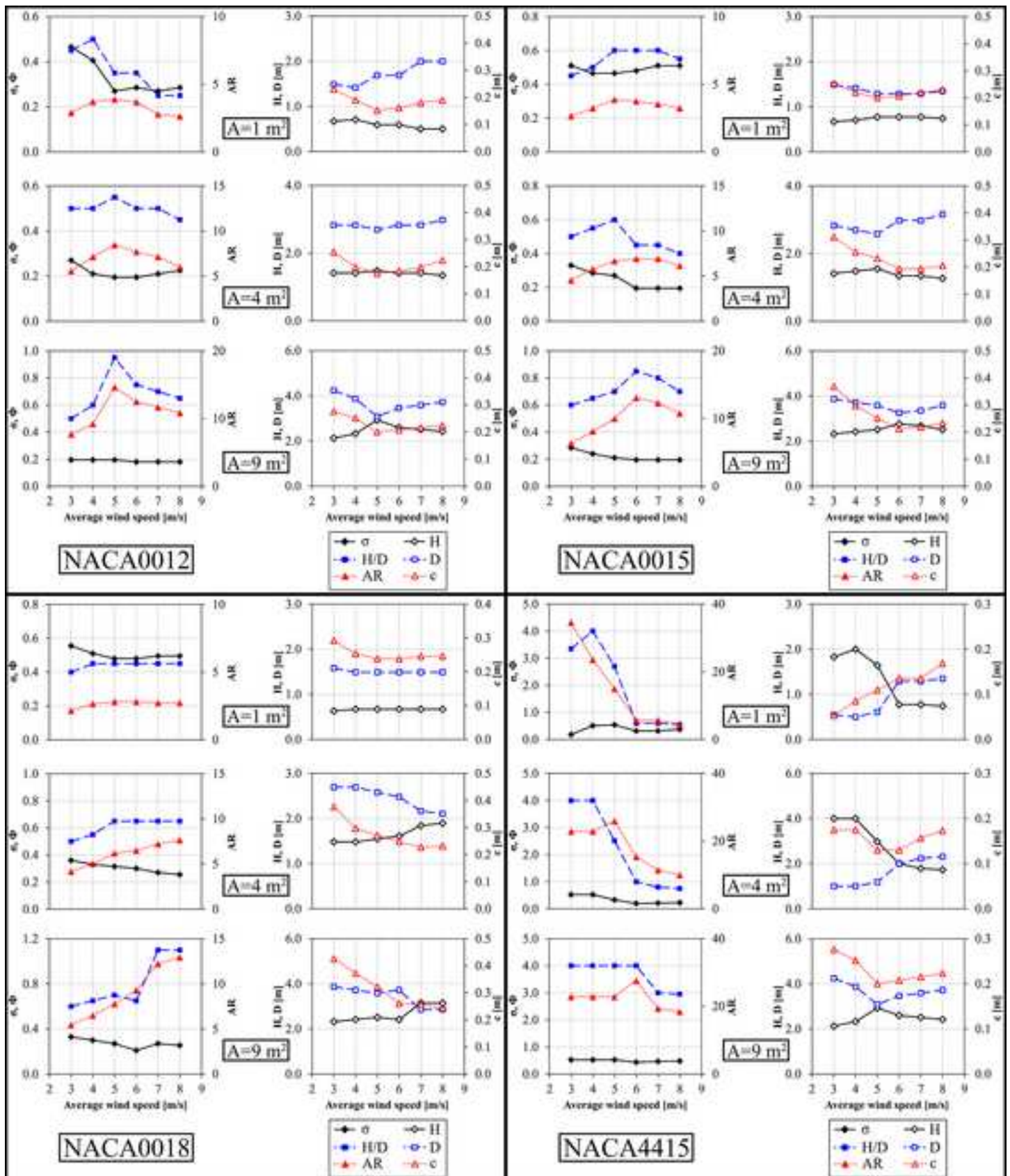
Parameter	Range/value
$\Phi=H/D$	0.25 - 0.50 - 0.75 - 1.00 - 1.50 - 2.00 - 2.50 - 3.00 - 3.50 - 4.00
$\xi=c/D$	0.005 - 0.015 - 0.025 - 0.050 - 0.075 - 0.100 - 0.125 - 0.150 - 0.175 - 0.200
A	1.0 - 4.0 - 9.0 [m ²]
Airfoils	NACA0012- NACA0015-NACA0018-NACA4415
\bar{U}	3 - 4 - 5 - 6 -7 - 8 [m/s]
Boundary conditions	Aerodynamics only / Centrifugal load / Struts' parasitic torque

Appendix A

[Click here to download high resolution image](#)







Optimal design configurations for Case 3

NACA 0012							
A=1 m ²							
\bar{U}	C/D	H/D	σ	AR	H	D	c
3	0.155	0.45	0.47	2.9	0.671	1.491	0.231
4	0.135	0.50	0.41	3.7	0.707	1.414	0.191
5	0.090	0.35	0.27	3.9	0.592	1.690	0.152
6	0.095	0.35	0.29	3.7	0.592	1.690	0.161
7	0.090	0.25	0.27	2.8	0.500	2.000	0.180
8	0.095	0.25	0.29	2.6	0.500	2.000	0.190
A=4 m ²							
\bar{U}	C/D	H/D	σ	AR	H	D	c
3	0.090	0.50	0.27	5.6	1.414	2.828	0.255
4	0.070	0.50	0.21	7.1	1.414	2.828	0.198
5	0.065	0.55	0.20	8.5	1.483	2.697	0.175
6	0.065	0.50	0.20	7.7	1.414	2.828	0.184
7	0.070	0.50	0.21	7.1	1.414	2.828	0.198
8	0.075	0.45	0.23	6.0	1.342	2.981	0.224
A=9 m ²							
\bar{U}	C/D	H/D	σ	AR	H	D	c
3	0.065	0.500	0.20	7.7	2.121	4.243	0.276
4	0.065	0.600	0.20	9.2	2.324	3.873	0.252
5	0.065	0.950	0.20	14.6	2.924	3.078	0.200
6	0.060	0.750	0.18	12.5	2.598	3.464	0.208
7	0.060	0.700	0.18	11.7	2.510	3.586	0.215
8	0.060	0.650	0.18	10.8	2.419	3.721	0.223

NACA 0015**A=1 m²**

Ū	C/D	H/D	σ	AR	H	D	c
3	0.170	0.45	0.51	2.6	0.671	1.491	0.253
4	0.155	0.50	0.47	3.2	0.707	1.414	0.219
5	0.155	0.60	0.47	3.9	0.775	1.291	0.200
6	0.160	0.60	0.48	3.8	0.775	1.291	0.207
7	0.170	0.60	0.51	3.5	0.775	1.291	0.219
8	0.170	0.55	0.51	3.2	0.742	1.348	0.229

A=4 m²

Ū	C/D	H/D	σ	AR	H	D	c
3	0.110	0.50	0.33	4.5	1.414	2.828	0.311
4	0.095	0.55	0.29	5.8	1.483	2.697	0.256
5	0.090	0.60	0.27	6.7	1.549	2.582	0.232
6	0.065	0.45	0.20	6.9	1.342	2.981	0.194
7	0.065	0.45	0.20	6.9	1.342	2.981	0.194
8	0.065	0.40	0.20	6.2	1.265	3.162	0.206

A=9 m²

Ū	C/D	H/D	σ	AR	H	D	c
3	0.095	0.60	0.29	6.3	2.324	3.873	0.368
4	0.080	0.65	0.24	8.1	2.419	3.721	0.298
5	0.070	0.70	0.21	10.0	2.510	3.586	0.251
6	0.065	0.85	0.20	13.1	2.766	3.254	0.212
7	0.065	0.80	0.20	12.3	2.683	3.354	0.218
8	0.065	0.70	0.20	10.8	2.510	3.586	0.233

NACA 0018**A=1 m²**

Ū	C/D	H/D	σ	AR	H	D	c
3	0.185	0.40	0.56	2.2	0.632	1.581	0.293
4	0.170	0.45	0.51	2.6	0.671	1.491	0.253
5	0.160	0.45	0.48	2.8	0.671	1.491	0.239
6	0.160	0.45	0.48	2.8	0.671	1.491	0.239
7	0.165	0.45	0.50	2.7	0.671	1.491	0.246
8	0.165	0.45	0.50	2.7	0.671	1.491	0.246

A=4 m²

Ū	C/D	H/D	σ	AR	H	D	c
3	0.140	0.55	0.42	3.9	1.483	2.697	0.378
4	0.110	0.55	0.33	5.0	1.483	2.697	0.297
5	0.105	0.60	0.32	5.7	1.549	2.582	0.271
6	0.100	0.65	0.30	6.5	1.612	2.481	0.248
7	0.105	0.85	0.32	8.1	1.844	2.169	0.228
8	0.110	0.90	0.33	8.2	1.897	2.108	0.232

A=9 m²

Ū	C/D	H/D	σ	AR	H	D	c
3	0.110	0.60	0.33	5.5	2.324	3.873	0.426
4	0.100	0.65	0.30	6.5	2.419	3.721	0.372
5	0.090	0.70	0.27	7.8	2.510	3.586	0.323
6	0.070	0.65	0.21	9.3	2.419	3.721	0.260
7	0.090	1.10	0.27	12.2	3.146	2.860	0.257
8	0.085	1.10	0.26	12.9	3.146	2.860	0.243

NACA 4415**A=1 m²**

Ū	C/D	H/D	σ	AR	H	D	c
3	0.060	3.35	0.18	34.5	1.830	0.546	0.053
4	0.170	4.00	0.51	23.5	2.000	0.500	0.085
5	0.180	2.70	0.54	15.0	1.643	0.609	0.110
6	0.105	0.60	0.32	5.7	0.775	1.291	0.136
7	0.105	0.60	0.32	5.7	0.775	1.291	0.136
8	0.125	0.55	0.38	4.4	0.742	1.348	0.169

A=4 m²

Ū	C/D	H/D	σ	AR	H	D	c
3	0.175	4.00	0.53	22.9	4.000	1.000	0.175
4	0.175	4.00	0.53	22.9	4.000	1.000	0.175
5	0.110	2.51	0.33	25.9	2.976	1.185	0.130
6	0.065	1.00	0.20	15.4	2.000	2.000	0.130
7	0.070	0.80	0.21	11.4	1.789	2.236	0.157
8	0.075	0.75	0.23	10.0	1.732	2.309	0.173

A=9 m²

Ū	C/D	H/D	σ	AR	H	D	c
3	0.175	4.00	0.53	22.9	6.000	1.500	0.263
4	0.175	4.00	0.53	22.9	6.000	1.500	0.263
5	0.175	4.00	0.53	22.9	6.000	1.500	0.263
6	0.145	4.00	0.44	27.6	6.000	1.500	0.218
7	0.155	3.00	0.47	19.4	5.196	1.732	0.268
8	0.160	2.95	0.48	18.4	5.153	1.747	0.279

Figure 1
[Click here to download high resolution image](#)

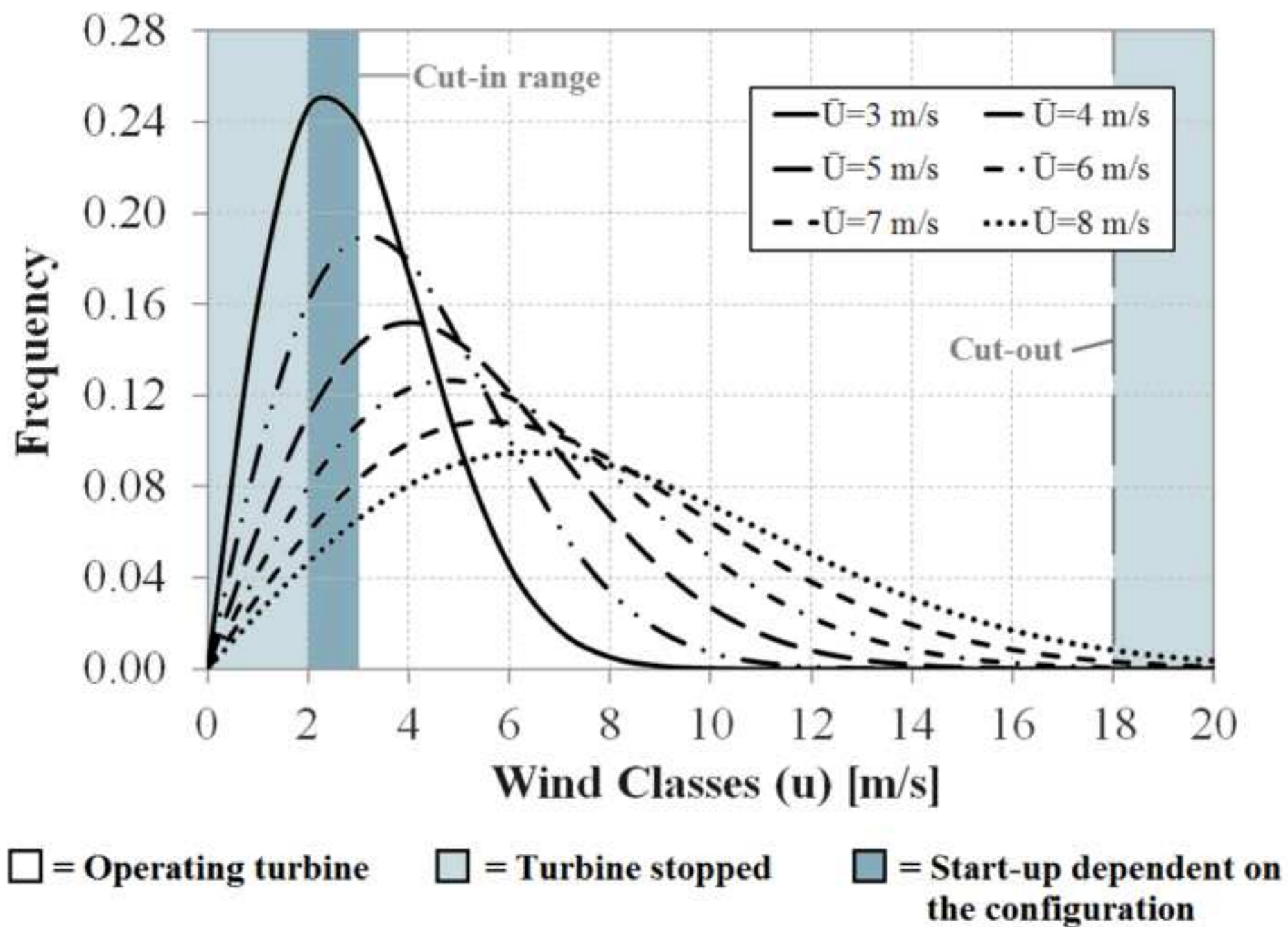


Figure 2
[Click here to download high resolution image](#)

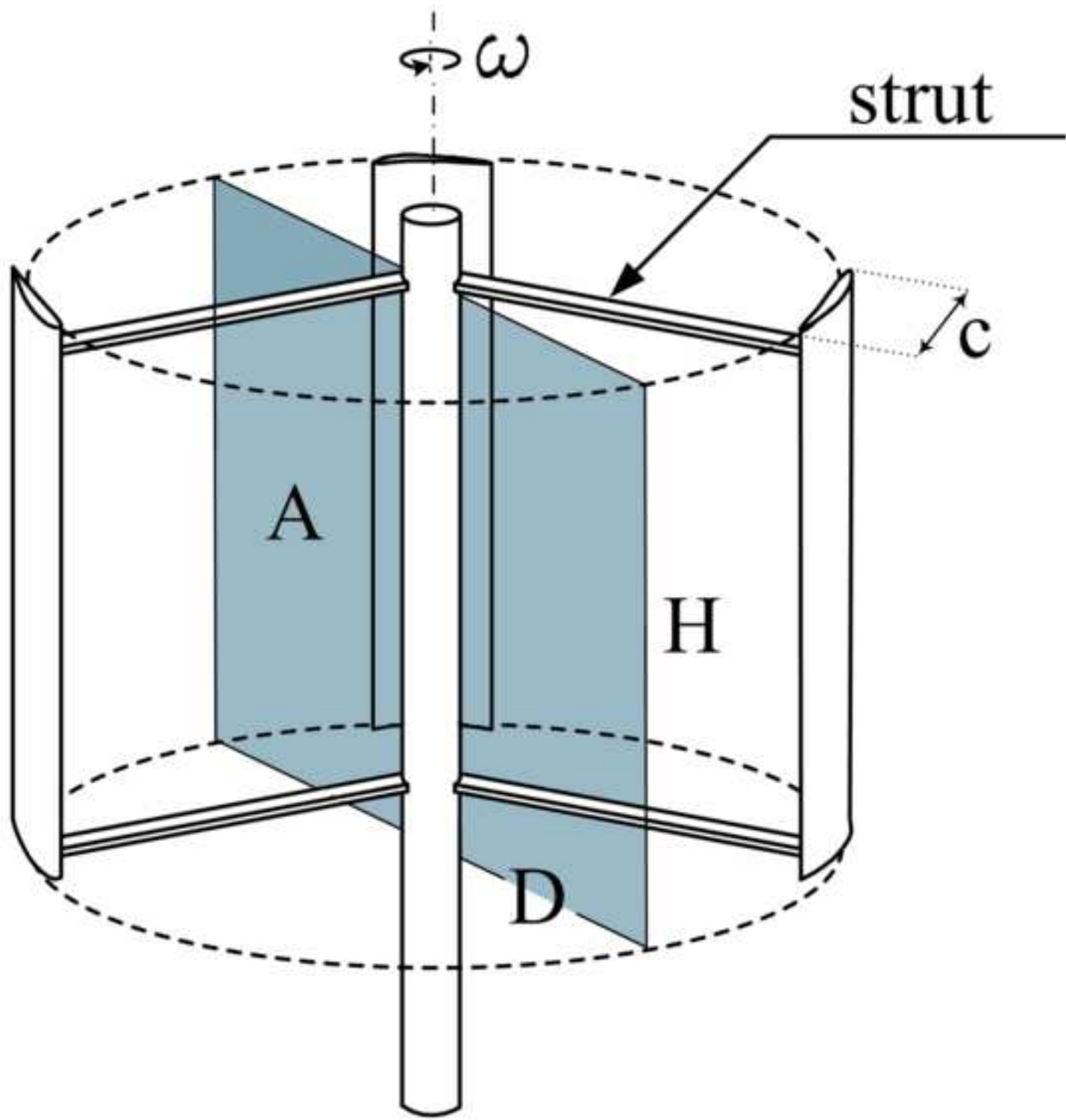


Figure 3
[Click here to download high resolution image](#)

NACA0018

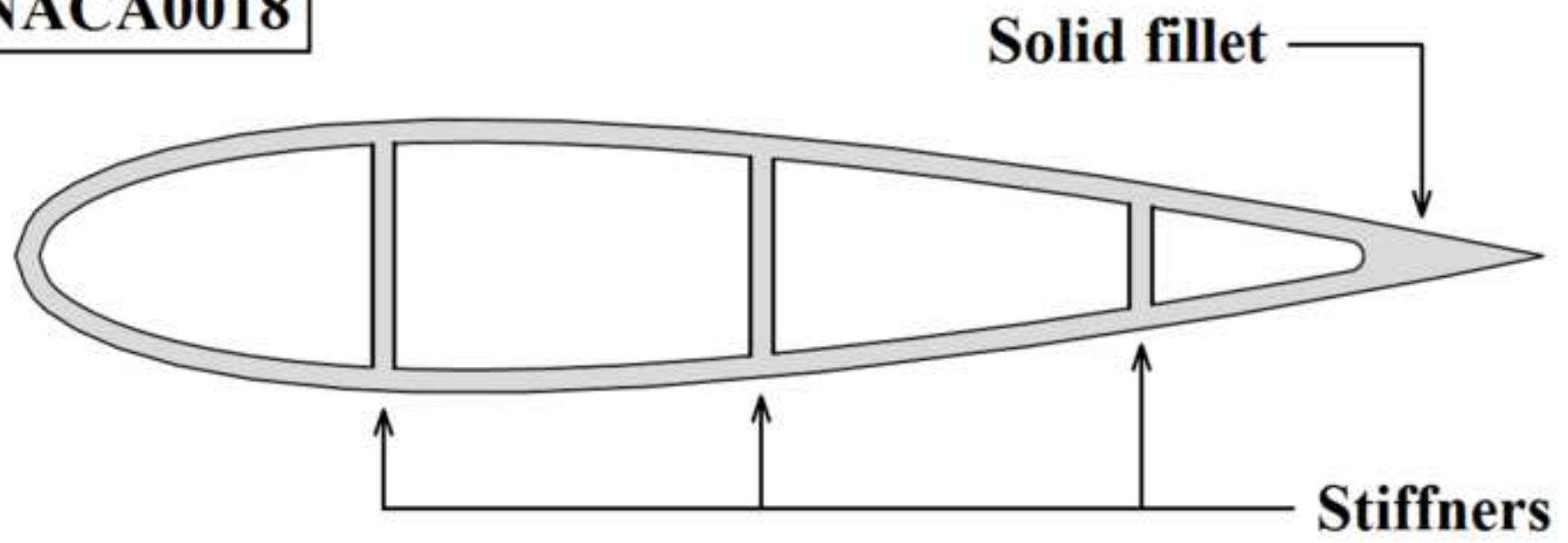
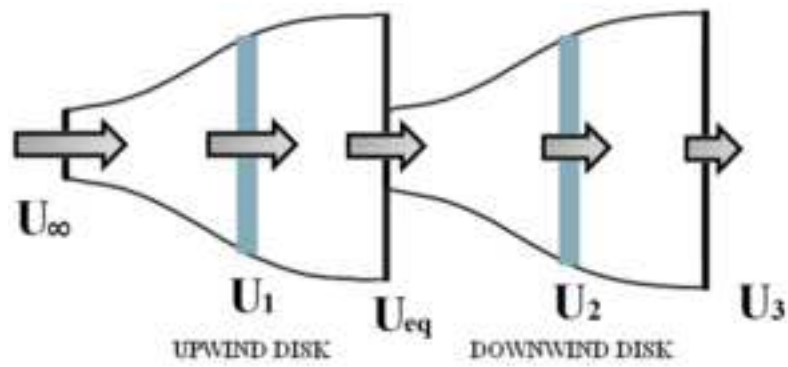
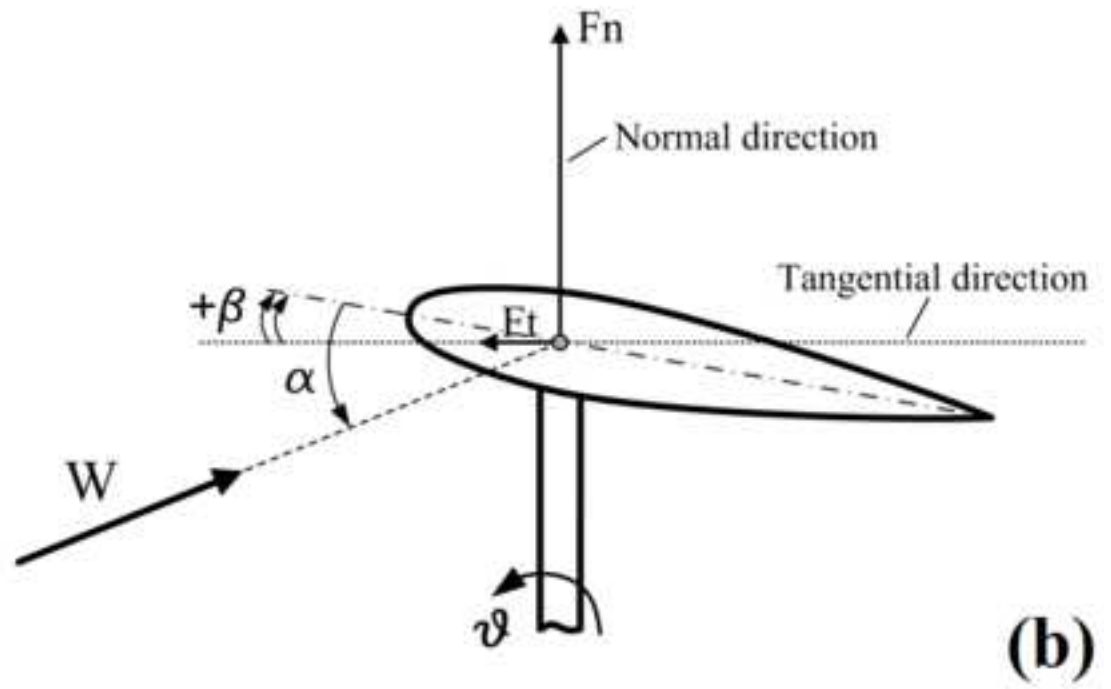
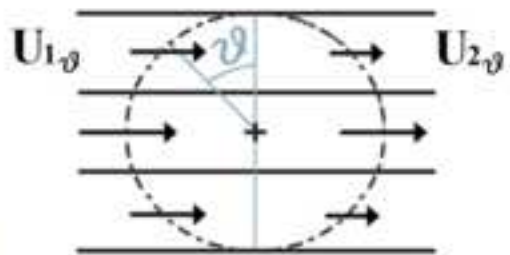


Figure 4
[Click here to download high resolution image](#)



(a)



(b)

Figure 5
[Click here to download high resolution image](#)

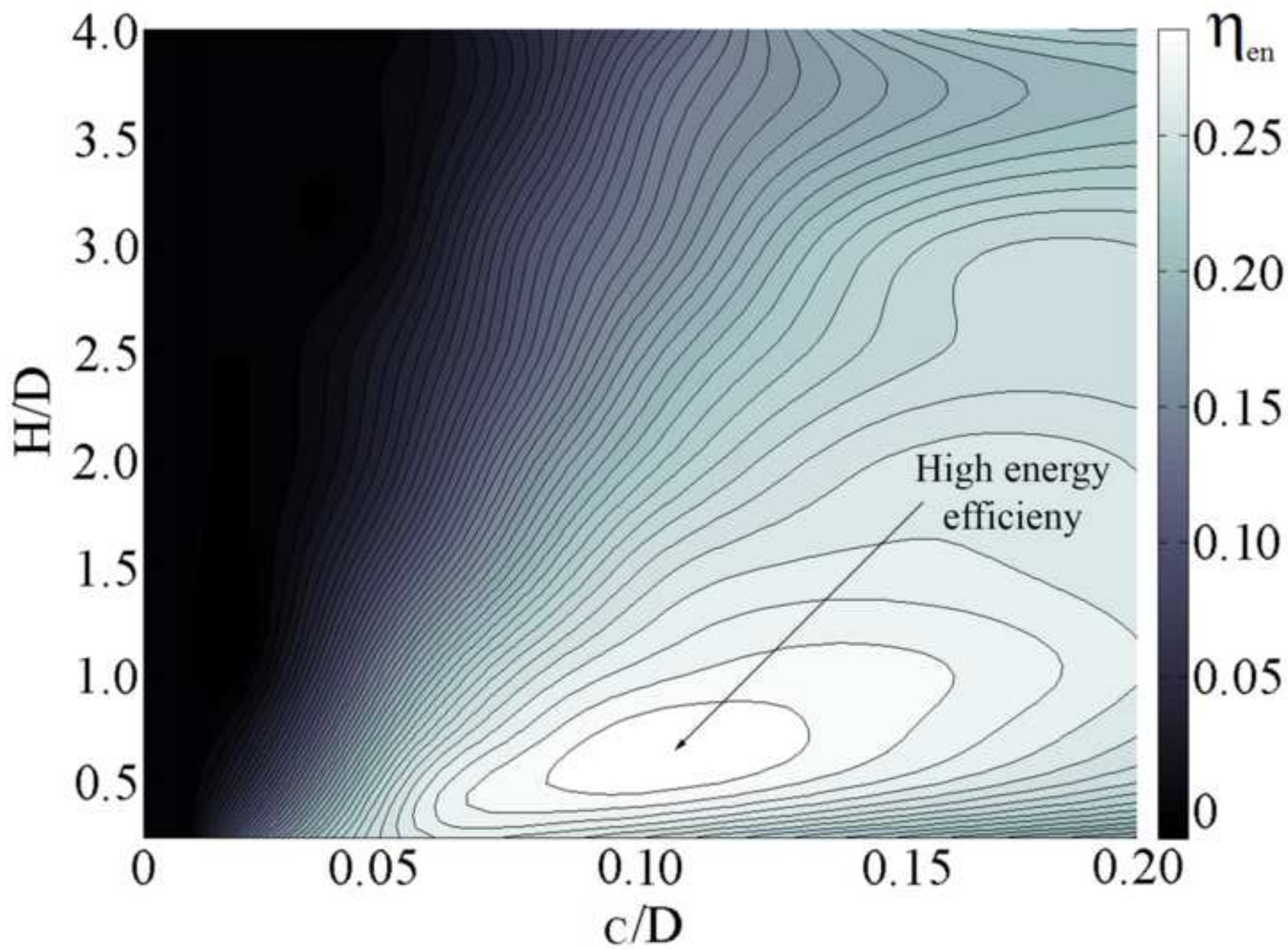


Figure 6
[Click here to download high resolution image](#)

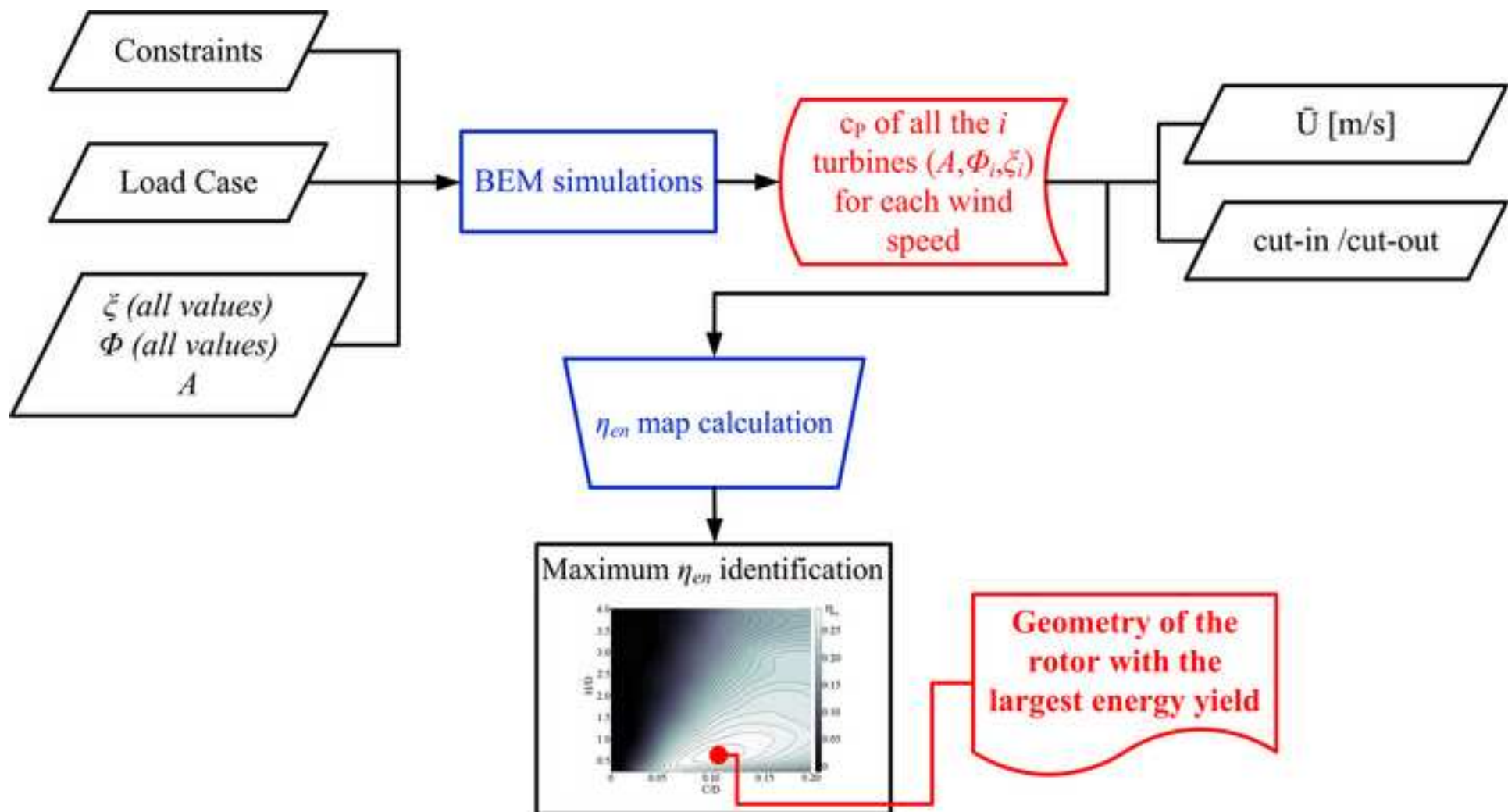


Figure 7

[Click here to download high resolution image](#)

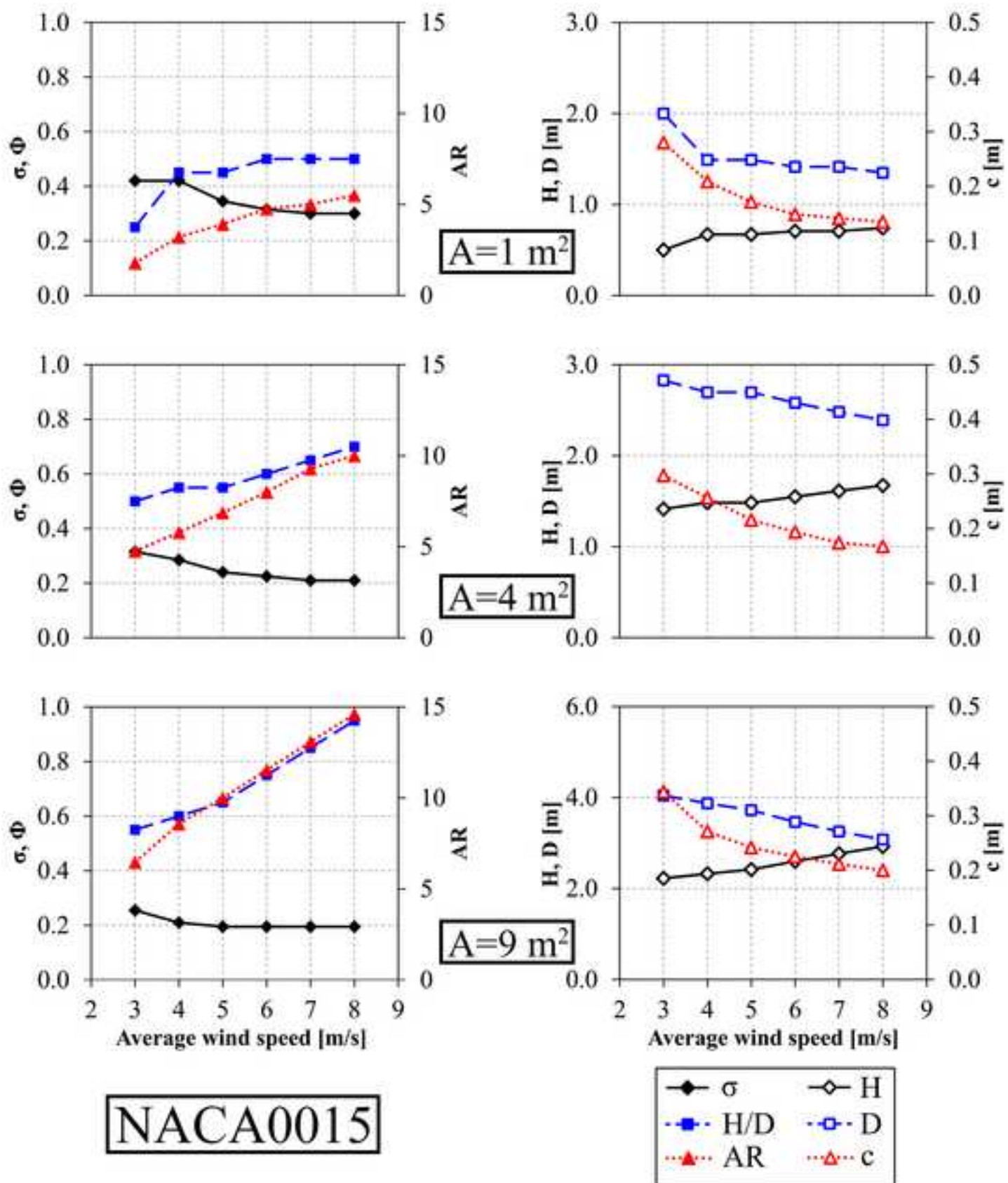


Figure 8
[Click here to download high resolution image](#)

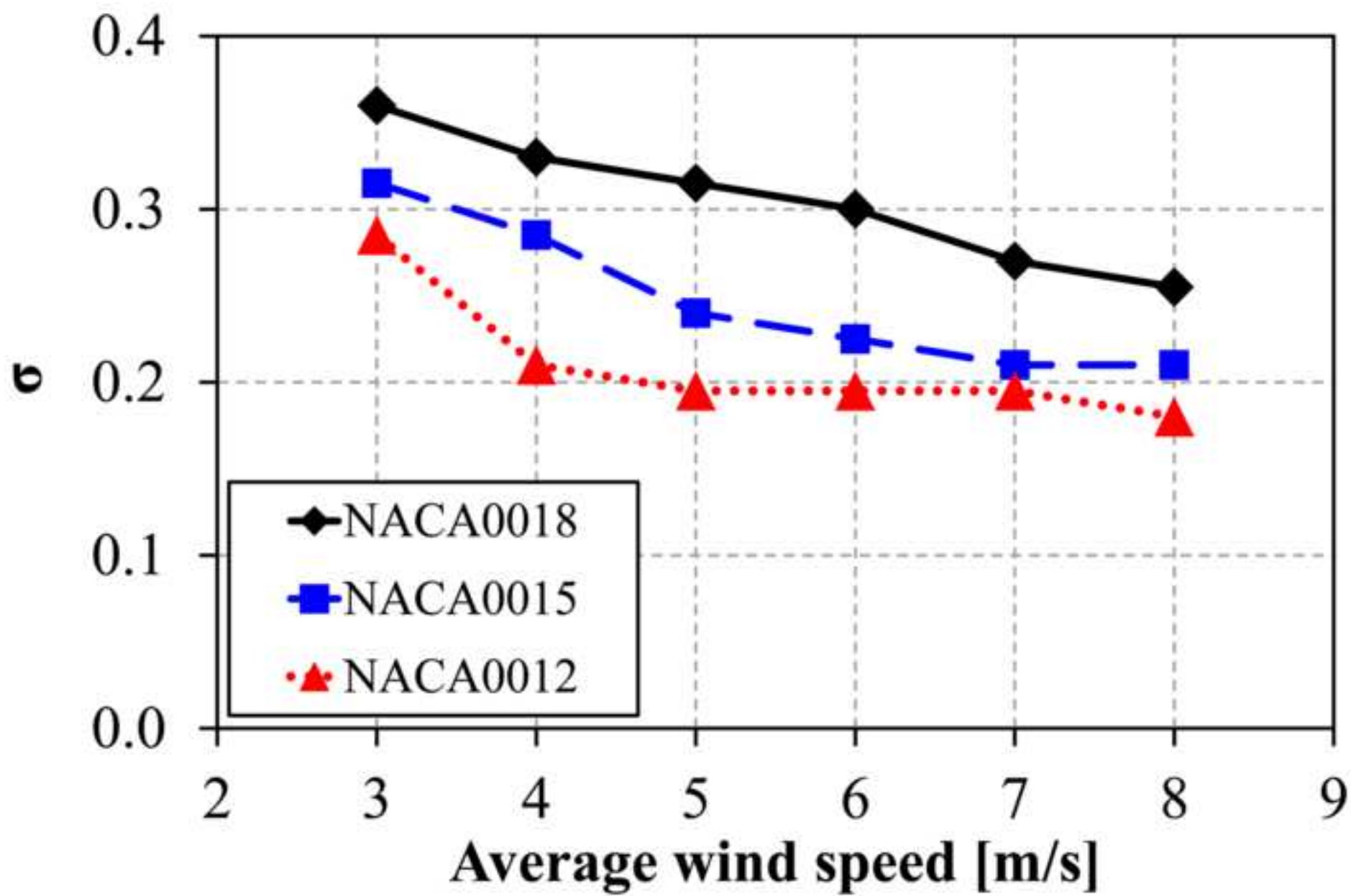


Figure 9
[Click here to download high resolution image](#)

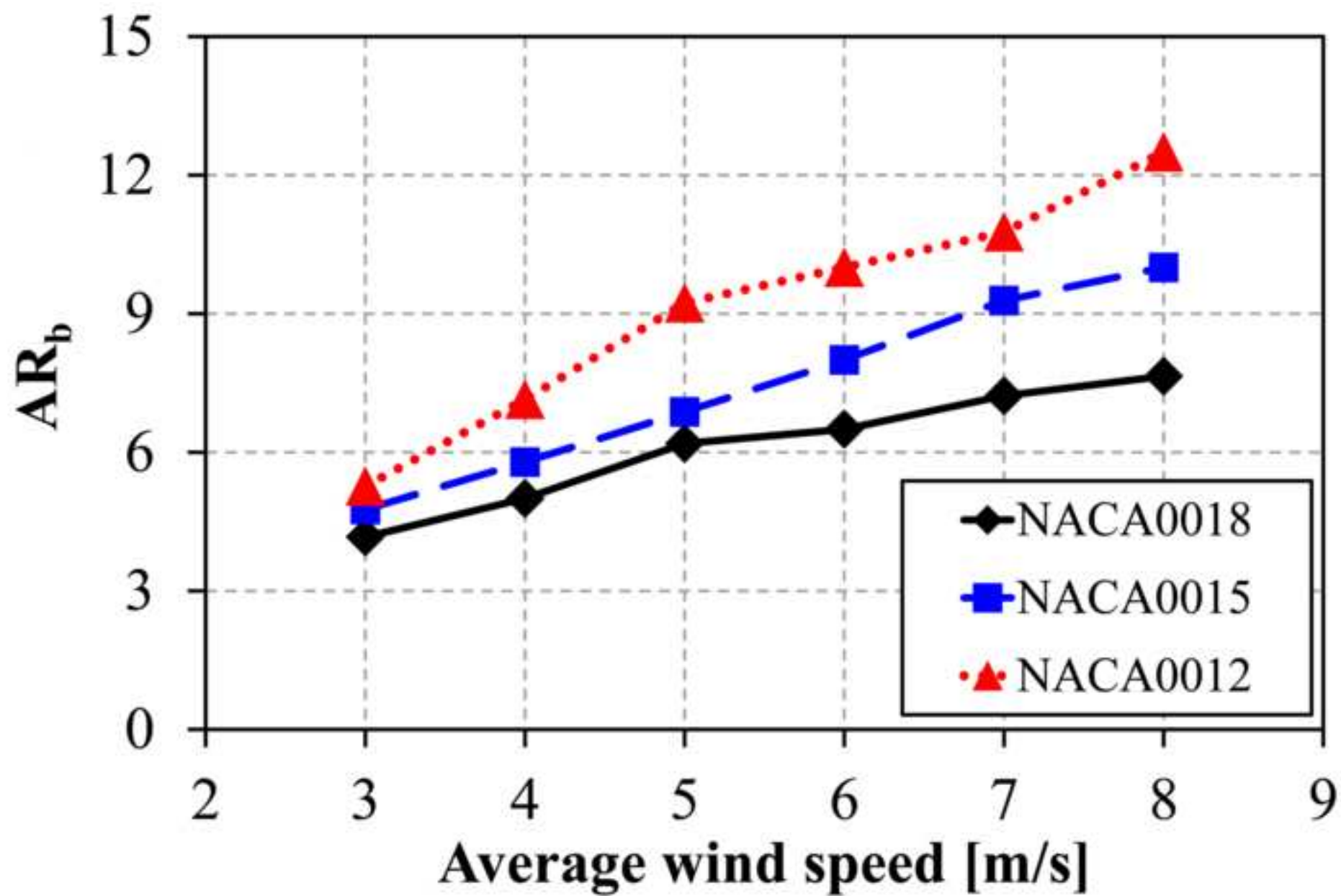


Figure 10
[Click here to download high resolution image](#)

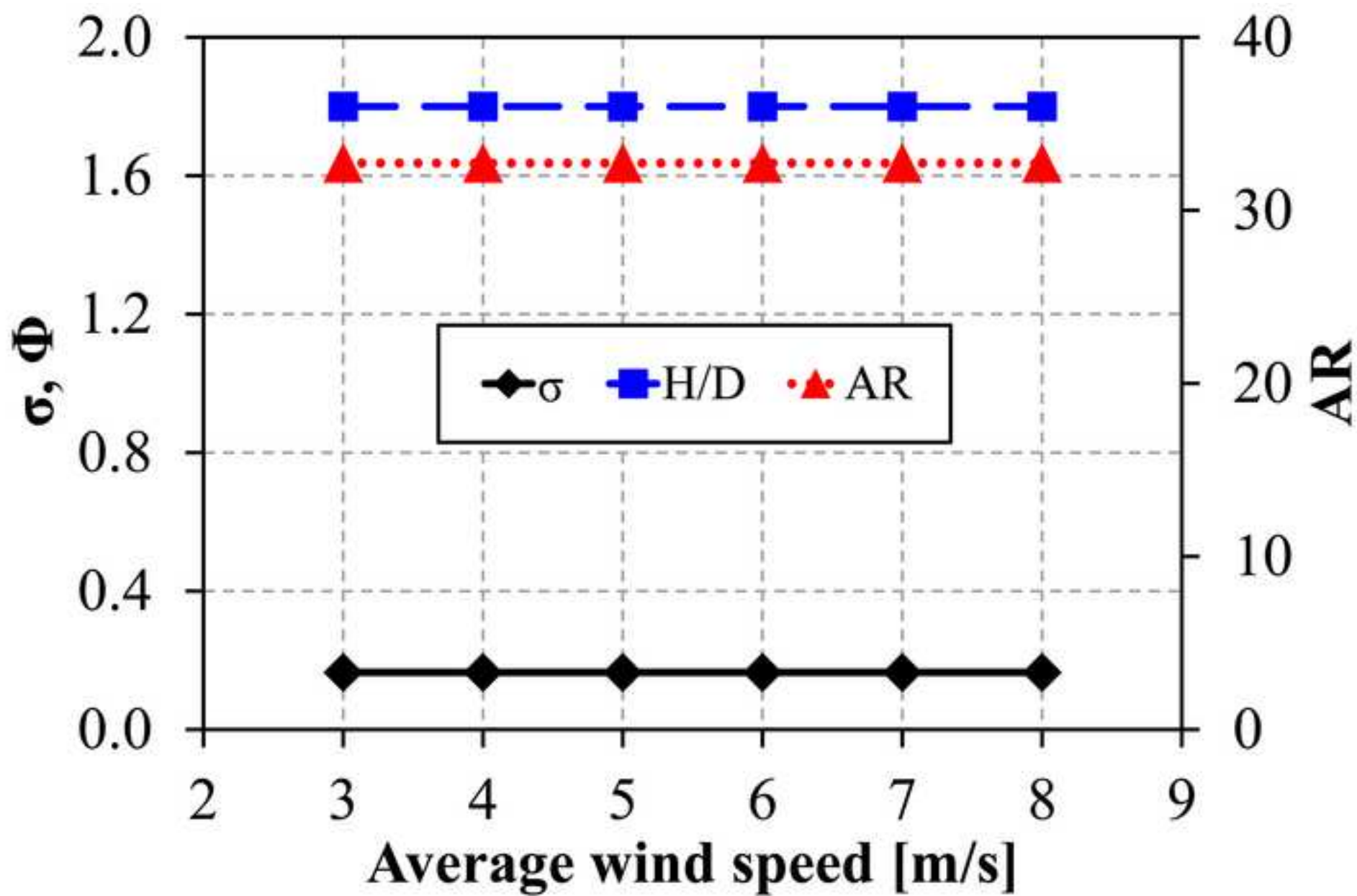


Figure 11
[Click here to download high resolution image](#)

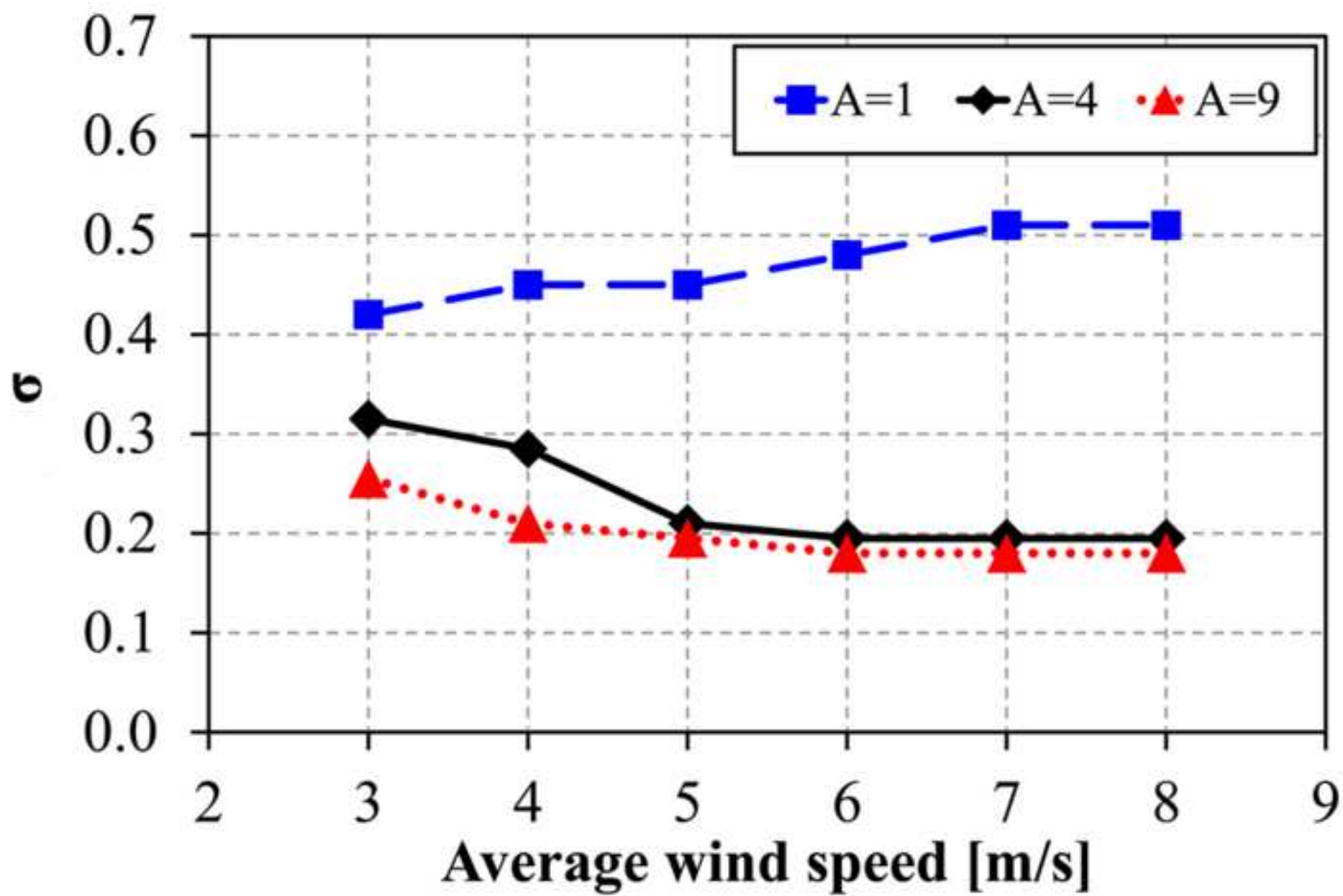


Figure 12
[Click here to download high resolution image](#)

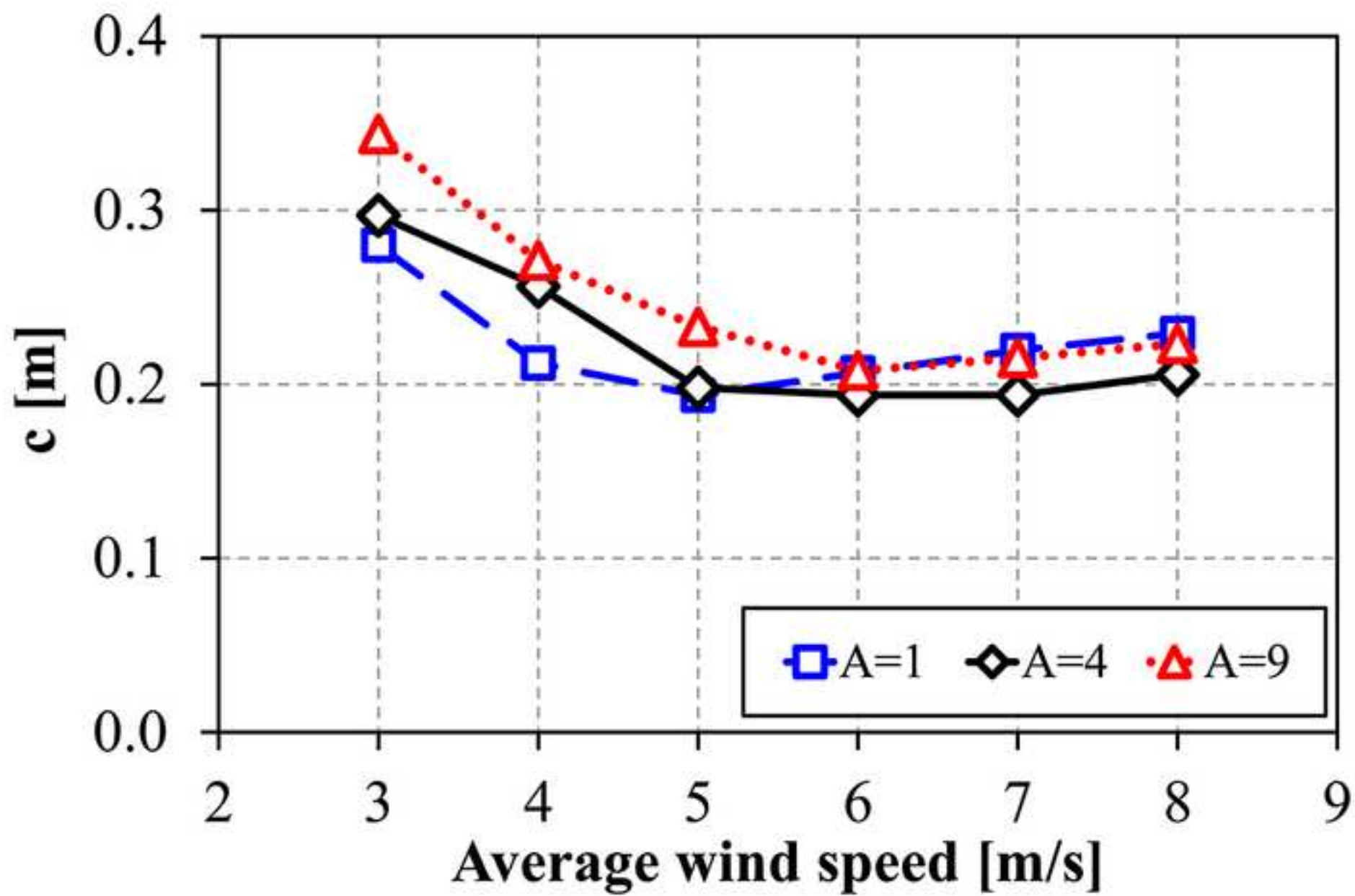


Figure 13

[Click here to download high resolution image](#)

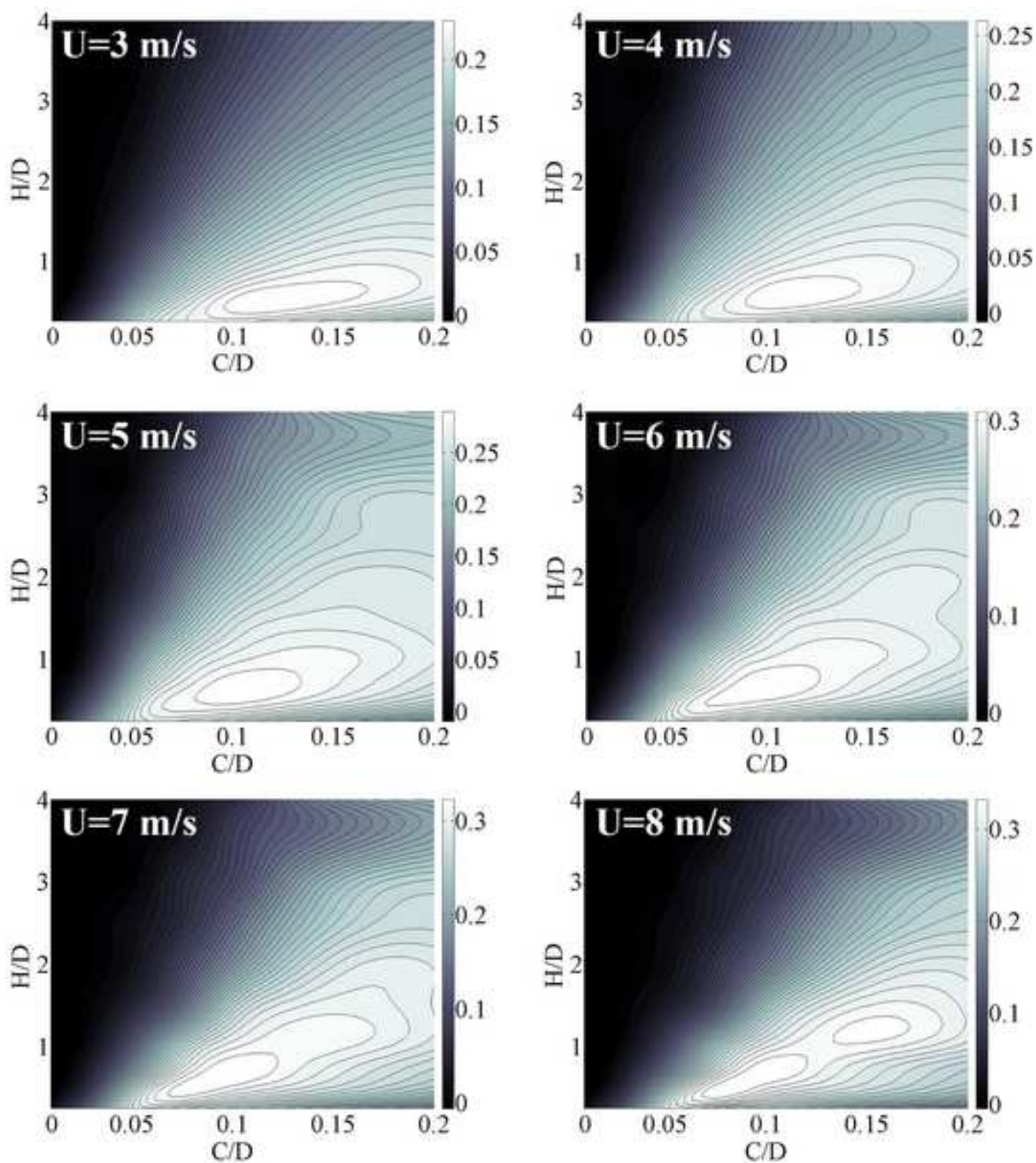


Figure 14
[Click here to download high resolution image](#)

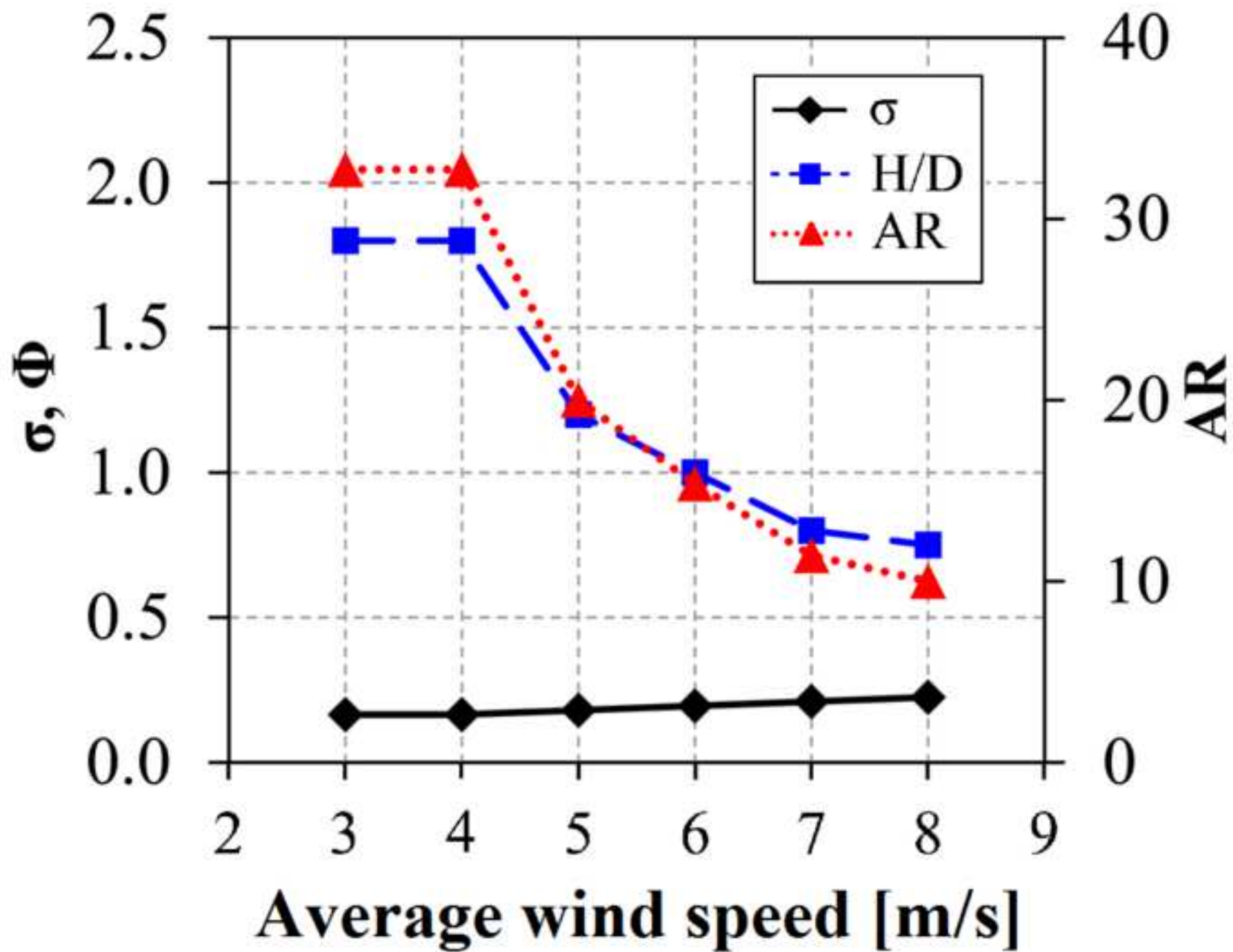


Figure 15

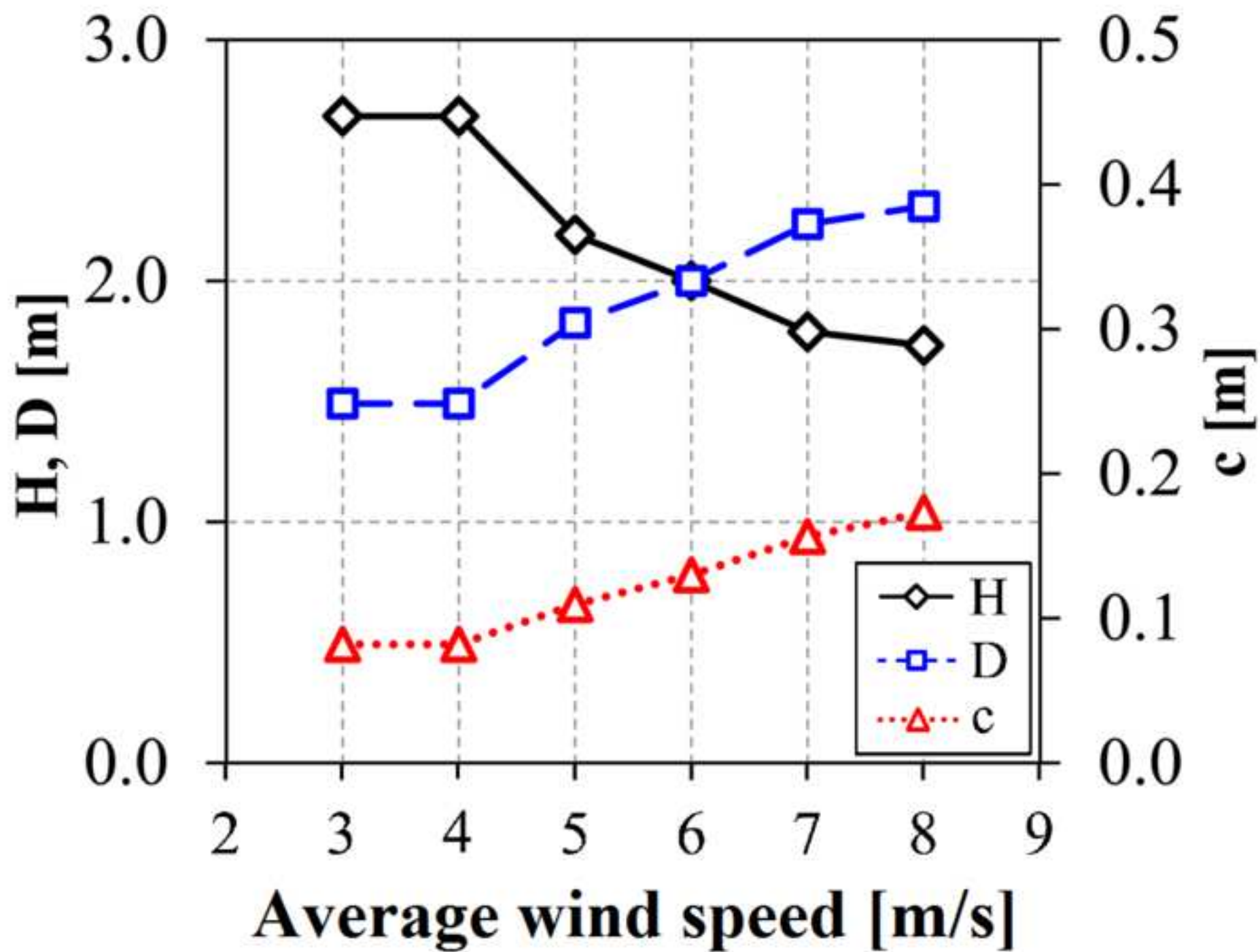
[Click here to download high resolution image](#)

Figure 16
[Click here to download high resolution image](#)

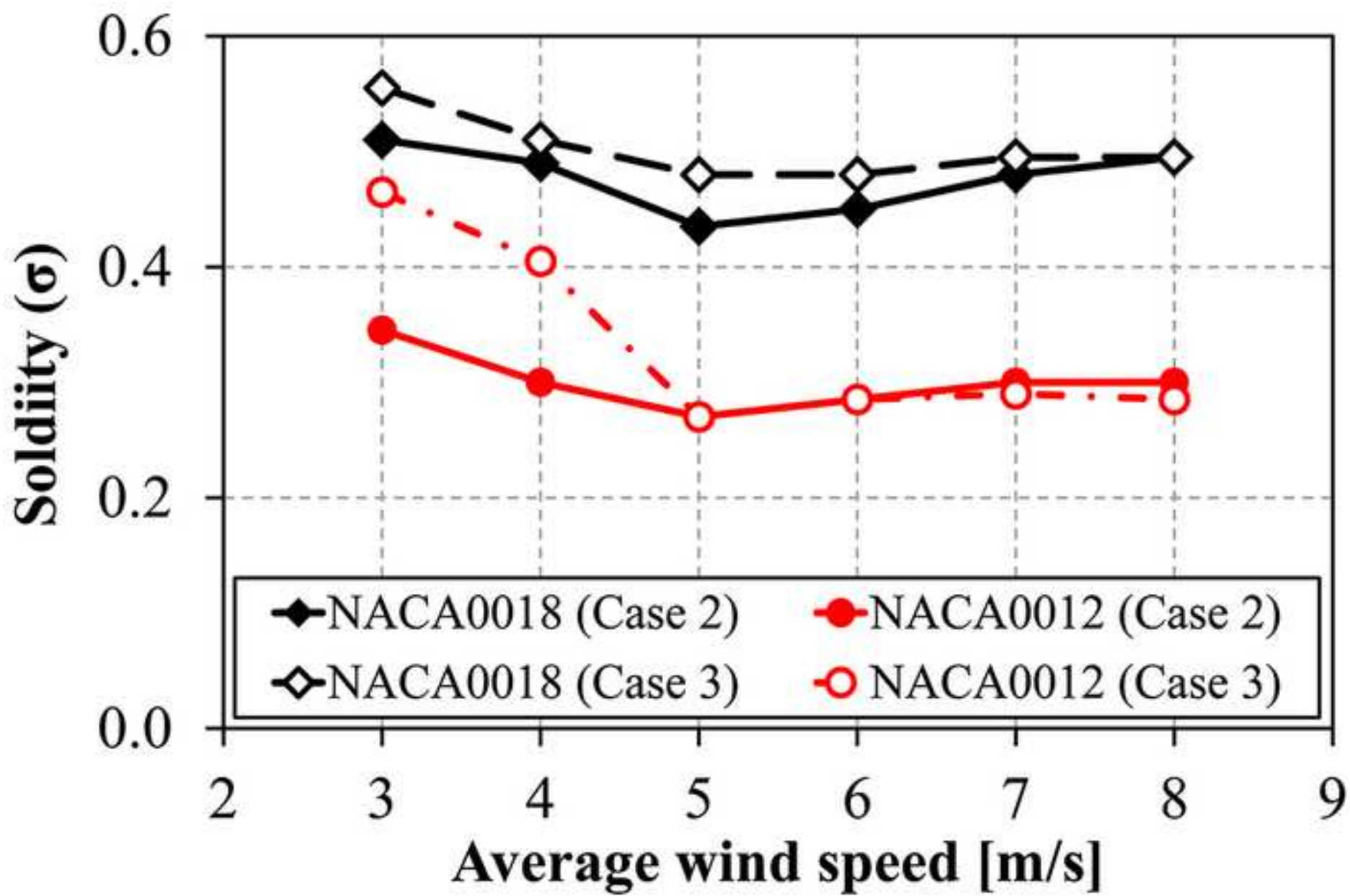


Figure 17
[Click here to download high resolution image](#)

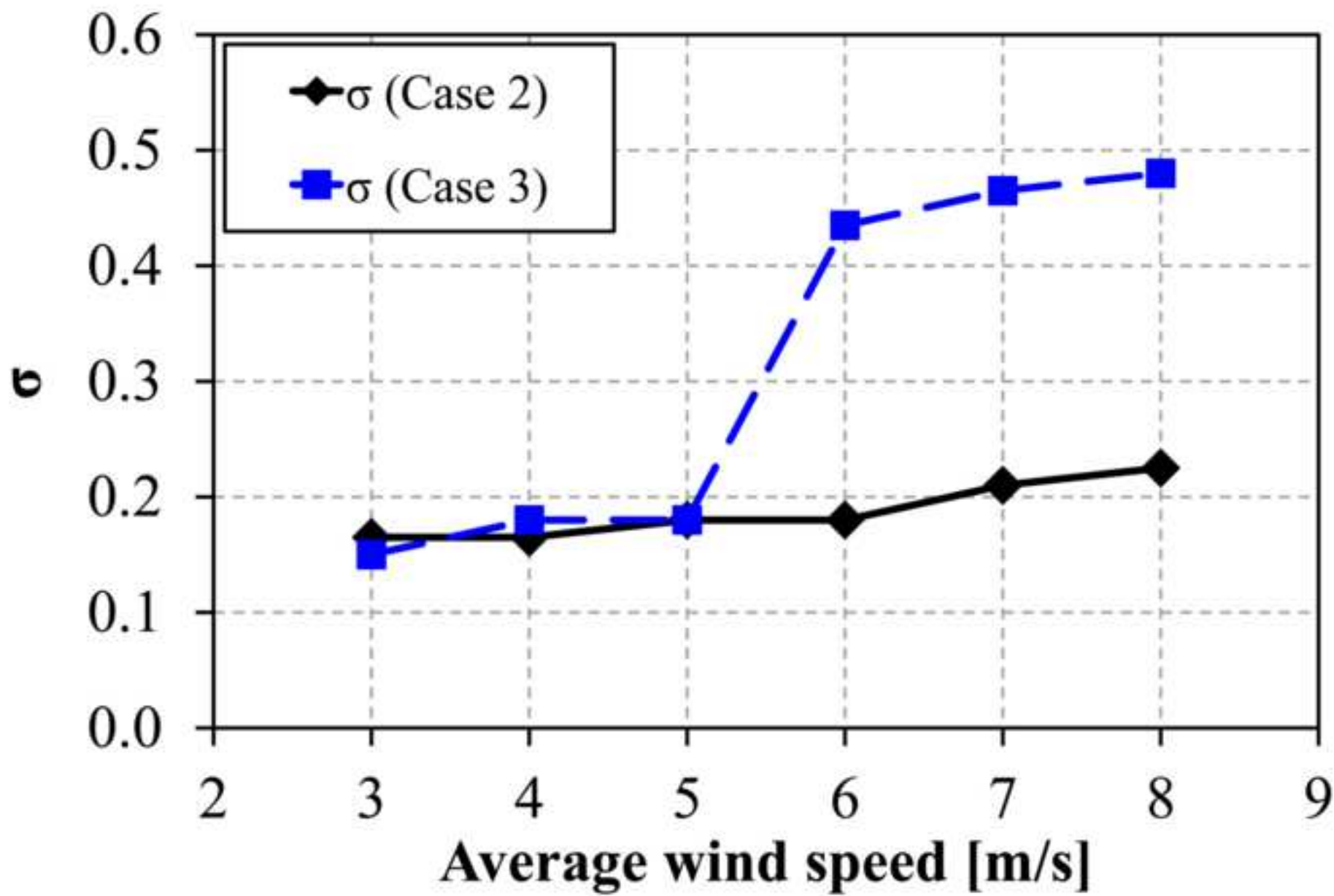


Figure 18

[Click here to download high resolution image](#)

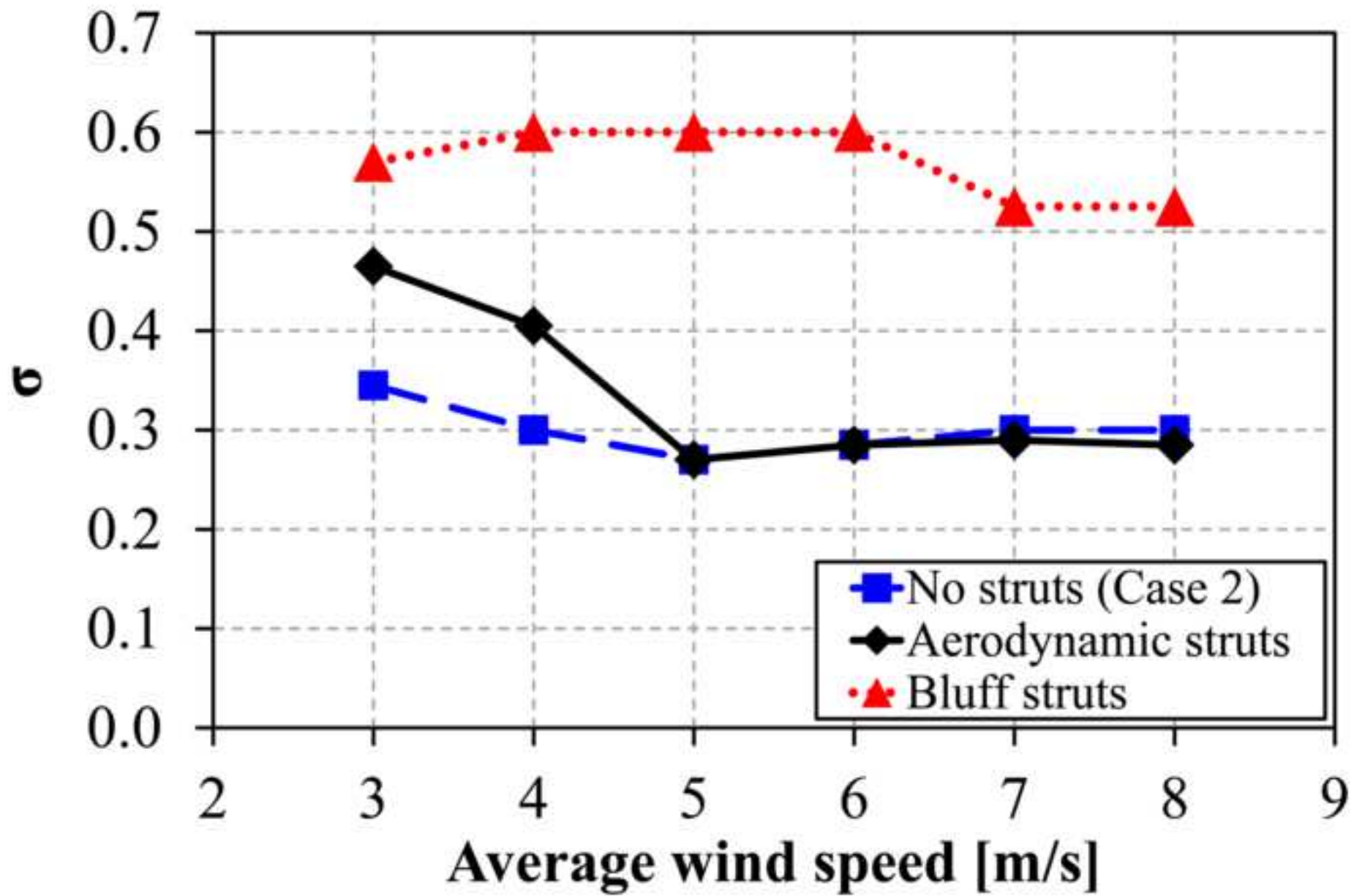


Figure 19
[Click here to download high resolution image](#)

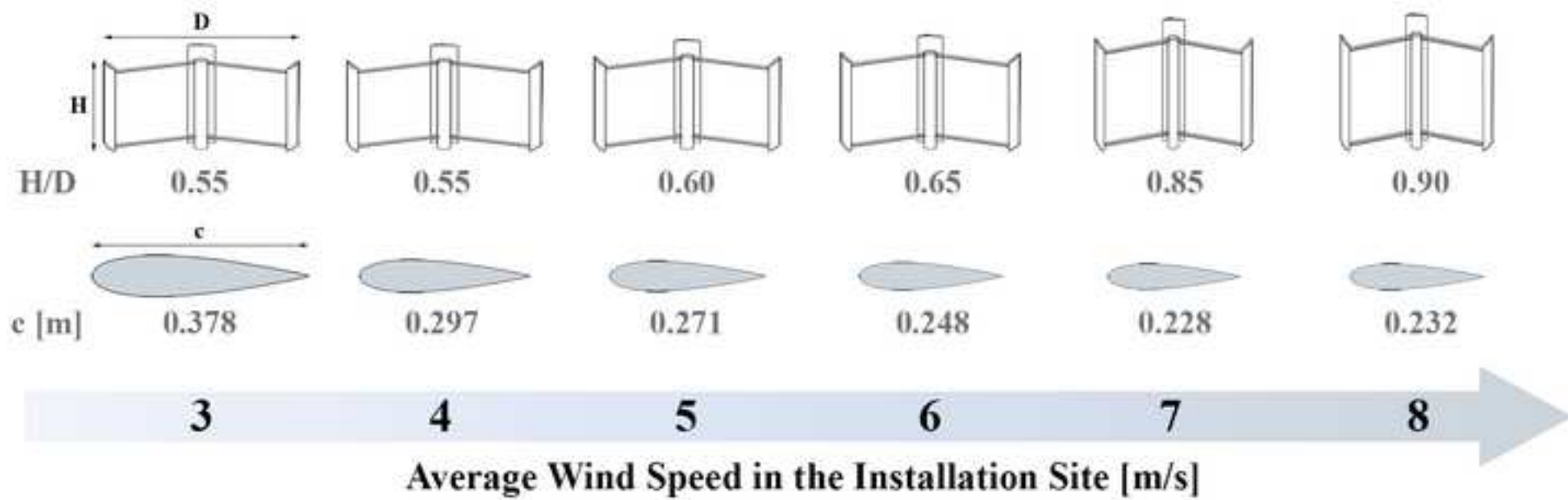


Figure 20
[Click here to download high resolution image](#)

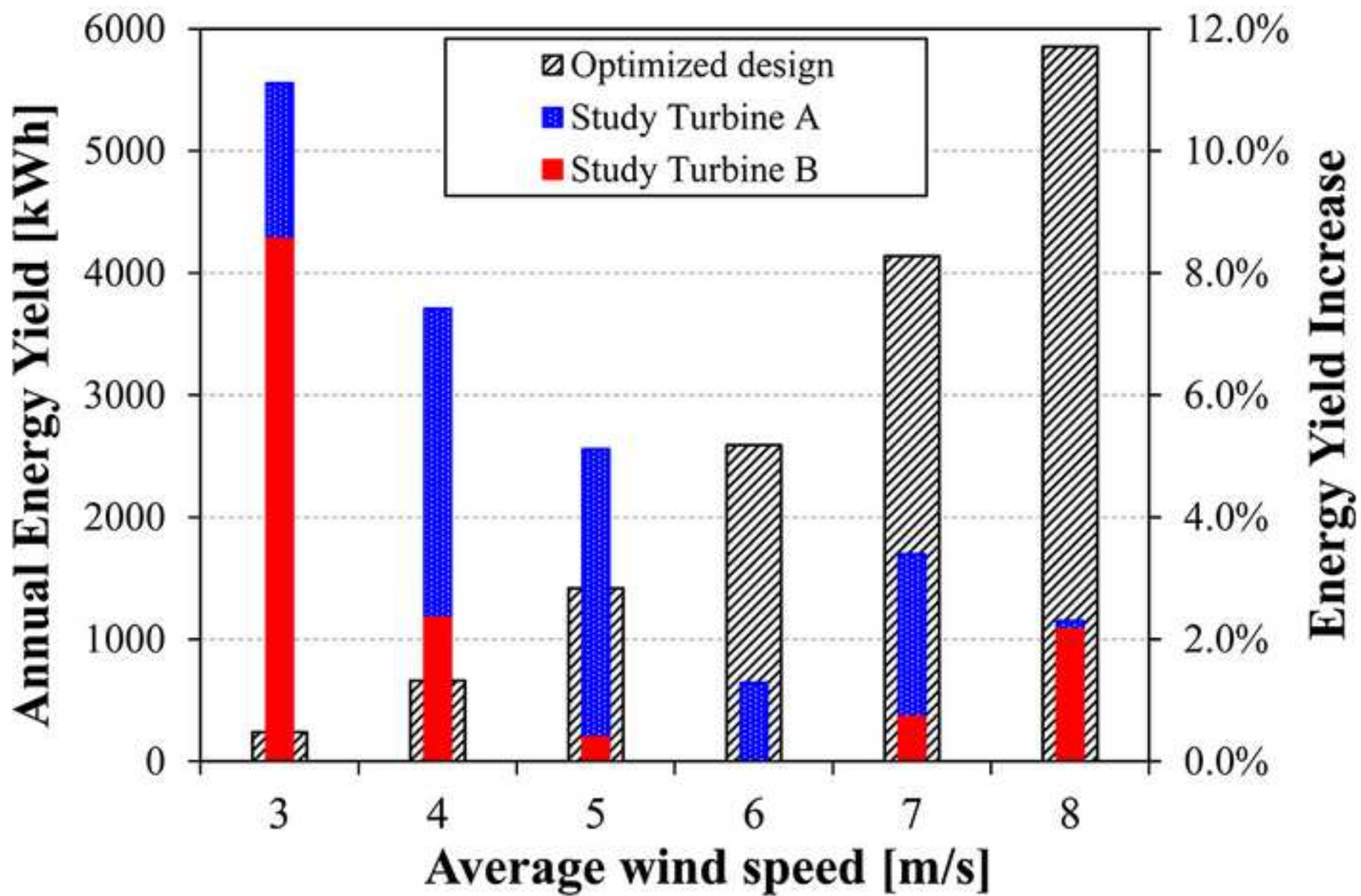


Figure 1 – Analyzed wind distributions coupled with the wind turbine functioning ranges.

Figure 2 – Schematic view of the architecture of the analyzed H-Darrieus turbines.

Figure 3 – Hypothesized manufacturing solution for the investigated airfoils (e.g. NACA0018).

Figure 4 - VARDAR code conventions. (a) Double Multiple Streamtubes approach; (b) Angle and forces conventions.

Figure 5 – Example of a calculated Energy Efficiency map: $A=4$, NACA0018, $\bar{U}=5$ m/s in Case 2.

Figure 6 - Procedure for the identification of the more energy-efficient rotor at each average wind speed.

Figure 7 – Trends of the most relevant design parameters (dimensional and dimensionless) for the solution with the maximum annual energy efficiency for different average wind speeds (NACA0015 airfoil in Case 1).

Figure 8 – Optimal design solidity for uncambered airfoils as a function of the average wind speed in Case 1.

Figure 9 – Optimal design AR_b for uncambered airfoils as a function of the average wind speed in Case 1.

Figure 10 – Optimum trends of the dimensionless design parameters of the turbine for the NACA4415 airfoil in Case 1.

Figure 11 – Optimal solidity for the NACA0015 airfoil as a function of the average wind speed and the swept area in Case 2.

Figure 12 – Optimal chord length for the NACA0015 airfoil as a function of the average wind speed and the swept area in Case 2.

Figure 13 - Migration of the maximum efficiency point as a function of the average wind speed for NACA0018, $A=4$ m² in Case 2.

Figure 14 - Optimal trends for the dimensionless parameters: NACA4415, $A=4$ m² in Case 2.

Figure 15 - Optimal trends for the dimensional parameters: NACA4415, $A=4$ m² in Case 2.

Figure 16 – Comparison between the optimal solidity trends in Case 2 and 3 for NACA0012 and NACA0018, $A=1$ m², as a function of the average wind speed.

Figure 17 – Comparison between the optimal solidity trends in Case 2 and 3 for NACA4415, $A=9$ m², as a function of the average wind speed.

Figure 18 – Effects of the parasitic torque of the struts on the optimal solidity trends: NACA0012, $A=1$ m².

Figure 19 – Turbine design based on the maximization of the annual energy yield. Best design solutions as a function of the average wind speed in the site for a rotor with a swept area of 4 m² and equipped with NACA0018 airfoils.

Figure 20 – Energy yields of the optimized turbines as a function of the average wind speed in the site ($A=4$ m² – NACA0018 airfoil).

Table 1 – Test-plan.

Florence, Italy
16/10/2014

Dear Prof. Al-Nimr,

based on the comments of Reviewer #2, we have completely revised both Figure 19 and the Graphical Abstract. Moreover, we have re-phrased the explanation of the figure in the paper and its caption. Our comments have been highlighted in blue both in this communication and in the revised version of the paper.

Best regards,

Alessandro Bianchini, Giovanni Ferrara, Lorenzo Ferrari

ooo ooo ooo

REVIEWER #1

The revised paper seems satisfactory and can be accepted

REVIEWER #2

In the modified paper, figure 19 is not comprehensible to me. Pl label the diagram properly so that difference among those rotor designs can be clearly understood. Further those wind speeds should have units as well. Also the same may be modified in the graphical abstract.

Based on the Reviewer's comment, we have completely revised both Figure 19 and the Graphical Abstract. To improve the clarity of the message of Figure 19, we have also rephrased its explanation in the paper and its caption.

REVIEWER #3

The corrections are made appropriately, please accept the manuscript.

23 The wind distributions were combined with the predicted performance maps of the rotors
24 obtained with a specifically developed numerical code based on a Blade Element Momentum
25 (BEM) approach. The influence on turbine performance of the cut-in speed was accounted for,
26 as well as the limitations due to structural loads (i.e. maximum rotational speed and maximum
27 wind velocity). The analysis, carried out in terms of dimensionless parameters, highlighted the
28 aerodynamic configurations able to ensure the largest annual energy yield for each wind
29 distribution and set of aerodynamic constraints.

30 **Keywords**

31 Darrieus, VAWT, wind turbine, design, energy yield, aerodynamics

32 **1. Introduction**

33 In 2011, the wind energy market grew by 6% compared to 2010, despite the economic and
34 political turmoil in Europe and North America, with a newly installed power of 40.5 GW [1].

35 The great bulk of installed wind energy plant is today in the form of large wind farms [2]
36 which mainly comprehend large Horizontal Axis Wind Turbines (HAWTs) feeding into power
37 supply grids: turbines are becoming more and more efficient and a scale-up tendency is clearly
38 distinguishable. Moreover, technological improvements in design and efficient maintenance
39 have considerably reduced their operating cost and consequently disclosed new diffusion
40 frontiers like the offshore applications [3-4]. Whereas these installations are a valuable addition
41 to the grid capacity, they actually do not benefit people who are not served by grids. As a
42 consequence, much interest is being paid to understand where wind turbines can effectively
43 represent an alternative for delocalized power production [5-6]. Paradoxically, however, there
44 has been very little research and commercial development in the second part of the century on
45 small stand-alone systems, although great improvements in the blade aerodynamic design have
46 been made. In recent times, a reversal of this trend has been fortunately experienced.

47 Increasing interest is especially being paid by architects, project developers and local
48 governments to understand where small wind turbines can effectively be exploited to provide
49 delocalized power in the built environment (e.g. see Refs. [7-12]). The real feasibility of this
50 scenario has, however, yet to be proved, both in terms of real energy harvesting and of
51 compatibility of the machines with a populated area [9-10,13].

52 In particular, Vertical-Axis Wind Turbines (VAWTs), both drag [14-16] and lift-driven [17-
53 20], are gaining popularity in the wind energy scenario, especially in medium and small-size
54 installations, where they can work effectively even in presence of low-speed and unstructured
55 flows with low noise emissions and high reliability. Among others, H-Darrieus rotors are
56 increasingly appreciated in unconventional contexts as they are even assumed to increase their
57 performance in case of an oncoming flow misaligned with respect to the axis of the rotor [17-
58 19]. In order to promote the diffusion of this technology, on one hand, industrial manufacturers
59 are developing new and more appealing design solutions (e.g. [21-25]); on the other hand,
60 efforts are being devoted to reducing the initial cost of the machines (primarily by means of
61 new materials) and to increasing the efficiency, in order to make them competitive with respect
62 to more conventional Horizontal Axis Wind Turbines (HAWTs) [20].

63 Focusing on the commercial aspects, it is also worth pointing out that almost all the industrial
64 rotors are generally designed and optimized for a specific wind speed (i.e. the speed which
65 ensures the highest energy production), but the rated power values, which are often perceived
66 by the final customer as the most valuable indicator of the quality of the product, are declared
67 for their nominal wind velocity, i.e. the highest functioning speed, which provides the
68 maximum power production. Although the importance of accounting for energy instead of
69 power does not come as a surprise for the applied-energy technicians, the implications of this
70 theoretical dichotomy are quite often not completely understood by the final customer of small
71 and medium wind turbines.

72 In detail, the actual operating conditions of a rotor over a year can indeed be very far from the
73 nominal one [9-10,26]. In particular, the available wind energy can be concentrated at the lower
74 wind velocities of the yearly distribution in the installation site, which can be often correctly
75 approximated by a Weibull function [27-30]; in addition, the specific features of the final
76 environment (e.g. local accelerations, effects of obstacles, etc.) are very important in
77 determining the real characteristics of the flow which effectively invests the rotor (e.g. [9-10]).
78 As a result, a turbine optimized only for a singular wind speed could provide poor performance
79 during the largest part of its operating time, with a remarkable reduction of the energy
80 produced and, consequently, of the suitability of the investment [10].

81 Stated the above, a design approach based on the maximization of the annual energy-yield
82 (i.e. the sum of the energy contributions at all the wind speeds experienced over the year) was
83 thought to represent a more valuable solution.

84 **2. Energy-yield-based design strategy**

85 The main goal of this study was to define some effective design guidelines for Darrieus wind
86 turbines which would be able to ensure the maximum energy harvesting in a yearly horizon as
87 a function of the attended wind distribution in the installation site.

88 With this goal in mind, 21600 test cases, i.e. permutations of a specific geometrical
89 configuration (300 cases), an airfoil (4 selections), a wind distribution (6 cases) and a load
90 system (3 cases), were tested and analyzed by means of a specifically developed numerical
91 code based on an advanced BEM method, in order to highlight the configurations which ensure
92 the largest annual energy yield for each wind condition.

93 **2.1 Wind distributions**

94 As a first step of the analysis, six annual wind profiles were hypothesized. As discussed, the
95 most logical representation of the annual wind distribution must be based on the assumption of
96 a Weibull distribution [27-30]. In particular, in the present study a constant shape factor equal

97 to 2.0 (Rayleigh distribution) was considered, whereas the scale factor was modified in each
98 case in order to ensure an average wind speed (\bar{U}) increasing by one from 3 to 8 m/s.

99 The choice of the Rayleigh distribution was based on literature data [9-10], which found that
100 this particular Weibull curve nicely approximates the wind distributions of some medium-low
101 velocity sites in Europe. The presented method, however, is of general validity and can be
102 applied to any Weibull distribution attended in the installation site.

103 In further detail, the wind profiles investigated in this study are shown in Figure 1, where the
104 cut-in and the cut-out limits are also displayed. In particular, it is worth pointing out that a
105 maximum cut-out velocity of 18 m/s was imposed for safety reasons to all the tested rotors
106 [26], based on the industrial experience for these rotors. On the other hand, the cut-in speed
107 was specifically calculated for each rotor on the basis of its behavior at low wind speeds: as
108 shown by Figure 1, a variable cut-in speed between 2 and 3 m/s was measured in the tested
109 rotors. In particular, it is worth pointing out that in the present study the attention was focused
110 only on the Darrieus machines, evaluating their actual self-starting characteristics. Although
111 recent studies (e.g. [31-32]) showed indeed that the self-starting can be enhanced by coupling
112 these rotors with drag-driven devices, the matching of the two turbines was not considered in
113 the scope of the present work and destined to further studies.

114 **2.2 Main design parameters for Darrieus-type turbines**

115 The proper set of rotor configurations to be analyzed was then defined. Due to the large
116 number of variables involved in the aerodynamic design of Darrieus rotors [20,26], some
117 preliminary assumptions were needed to focus the analysis on a significant family of turbines.

118 In particular, the following main choices were made:

- 119 ■ The H-Darrieus configuration with straight blades was selected (see Figure 2). This turbine
120 shape is presently the most exploited and studied solution in Darrieus turbines design, due
121 to higher efficiency and lower manufacturing costs with respect to original troposkien-
122 bladed rotors [20,24,33].

149 would consist in a direct increase of the chord c (Eq. 1). This solution is definitely able to
150 accomplish the goal, but strict limitations to its use must be introduced. In particular, notably
151 longer chords produce both a reduction of the Aspect Ratio of the blade (i.e. the ratio between
152 the blade length and the chord - Eq. 2) and an increase of the solidity of the rotor (Eq. 3)
153 [21,24,26].

$$154 \quad AR_b = \frac{H}{c} \quad (2)$$

$$155 \quad \sigma = \frac{Nc}{D} \quad (3)$$

156 The first effect actually results in a detriment of the blade efficiency [18,21], as the increase
157 of the rotor's height to compensate cannot be always provided as the swept area of the rotor is
158 generally a priori selected (Eq.4 for an H-Darrieus).

$$159 \quad A = H \cdot D \quad (4)$$

160 On the other hand, an increase of the solidity also produces a reduction of the peak efficiency
161 of the rotor [20,21,24], which once more cannot be simply compensated by reducing the
162 diameter because this countermeasure would directly reduce the peripheral speed, thus leading
163 to an undesired reduction of the relative speed W (given by the vector sum of the peripheral
164 speed and the wind speed reduced by the induction factor a - see Eq.5):

$$165 \quad W = \omega R + U(1 - a) \quad (5)$$

166 The second way to control the Reynolds number on the blade is in fact the modification of the
167 relative speed. Having assumed that the wind speed U is fixed, the only way to modify w is
168 related to a variation of the peripheral speed ωR .

169 Analogous to the previous analysis a double choice is given. An increase of the turbine radius
170 would directly improve the Reynolds number: being A fixed, the turbine's height would be
171 reduced (Eq. 4) and then the Aspect Ratio of the blades (Eq.2), leading to less efficient blades.
172 On the other hand, increasing the revolution speed would improve the relative speed, having,

173 however, a notable impact on the incidence angles range and the structural behavior of the
174 rotor.

175 Based on the above, the influence of the selected parameters can be readily highlighted.

176 ▪ **Φ ratio** - The Φ ratio has a double effect in defining the features of the rotor. From an
177 aesthetic point-of-view, it can be considered as a “shape factor” of the turbine, i.e. an
178 indicator of the visual proportions of the virtual cylinder swept during the revolution. On
179 the other hand, for a fixed swept area, low Φ values are typical of a machine in which the
180 optimal flow conditions on the airfoil are obtained thanks to large diameters in order to
181 increase the peripheral speed. In this configuration, the velocity triangles on the airfoils are
182 improved but the blades are generally short, with more relevant losses due to end-effects.
183 Conversely, high Φ values can be related to machines in which the efficiency of the blade
184 (high blade Aspect Ratios - Eq. 2) is preferred.

185 ▪ **ζ ratio** - The c/D ratio is a direct indicator of the solidity (σ) of the rotor (Eq. 3). High
186 values of ζ generally indicate that the chord length is increased to improve the Reynolds
187 number, whereas low ζ values can be related to rotors in which the relative wind speed is
188 increased by means of an increase of the relative wind speed on the airfoil (Eq. 5).

189 ▪ **Swept Area (A)** - As one can argue from the previous discussion, the swept area of the
190 turbine (Eq. 4 - valid for an H-Darrieus rotor) is unfortunately a dimensional parameter
191 which cannot be bypassed in the analysis of small rotors. In particular, larger swept areas
192 ensure less demanding limits of the turbine’s radius, ensuring higher peripheral speed and,
193 therefore, fewer problems in ensuring a good Reynolds number on the blades. Moreover,
194 being the optimal solidity ranges generally constant [20-21], the minimum requested
195 chords are generally smaller, resulting in higher Aspect Ratios and more efficient blades.

196 ▪ **Design variables** - The airfoil type is very important in defining the performance of a
197 Darrieus turbine; as a result, the dimensionless analysis on the best design trends must be
198 individually carried out for each specific airfoil family [20,34-35]. Finally, the struts’

199 shape and dimensions must be carefully taken into account as they can substantially
200 modify the power output of an H-Darrieus rotor (see Refs. [21,24,33,36]) due to the
201 parasitic torque that is produced during the revolution. To this purpose, the impact of the
202 struts was also included in this study by assuming a variation of their dimensions, and even
203 number, as a function of the structural stresses on the blades.

204 **3. Test plan and design parameters**

205 The test plan of the investigated configurations is summarized in Table 1.

206 The limits of the ζ and Φ parameters were defined on the basis of a survey of the technical
207 literature (e.g. [5,20,24]). In particular, the ξ range was limited to 0.200 as higher values would
208 lead to solidities higher than 0.6. Design choices over this limit are in fact considered to be
209 unsuitable for H-Darrieus rotors [20,24], due to the fact that the turbine is deemed to become
210 similar to a solid obstacle for the wind and the interactions between upwind and downwind
211 blades becomes so strong to compromise the aerodynamics of the airfoils. In addition, the
212 theory applied in the simulations could become less predictive in similar test-cases [20].

213 The choice of the aerodynamic airfoils was also based on a literature survey [5,20-21]. In
214 particular, four different airfoils were investigated in this work, in order to highlight the impact
215 of their aerodynamic characteristics on the effective energy harvesting of the turbine. The
216 airfoils were selected among the 4-digit NACA family, which is quite a conventional solution
217 in Darrieus VAWTs [5,20,34-35].

218 In detail, three uncambered airfoils with different thickness/chord ratios (NACA0012,
219 NACA0015, NACA0018) were compared to an asymmetrical and lightly-cambered airfoil
220 (NACA4415). The first group of airfoils is a widely exploited solution in Darrieus turbines, as
221 it ensures a suitable resistance to the stall coupled with good lift outputs at medium-range
222 Reynolds numbers. Moreover, a symmetric airfoil is able to provide the same lift contribution
223 either with positive or negative incidence [20,24]. On the other hand, a cambered profile, like
224 the selected NACA4415, has been suggested in technical literature (e.g. see [5,21]) as an

225 interesting design choice in order to ensure high peak values of the torque in low-velocity
226 cases, although some doubts on their effective application are due to the different behaviour of
227 a non-symmetric airfoil in case of a positive or negative incidence [21].

228 Focusing on the boundary conditions in terms of loads applied to the rotor, three different
229 configurations were analyzed:

230 ▪ **CASE 1 – Aerodynamics only:** in this configuration, the contribution of the resistant
231 torque of the struts was not considered. By doing so, this configuration actually refers to a
232 hypothetical solution of a fully aerodynamic relationship between the geometrical features
233 of the rotor and the power performance. Although not practically applicable, the analysis
234 of these results allows one to define the aerodynamic trends and to directly compare the
235 functioning behavior of machines having different areas. Moreover, by defining the purely
236 aerodynamic requests, one can also directly identify the effects induced by the secondary
237 and parasitic effects due to auxiliary organs (e.g. the struts) and external loads.

238 ▪ **CASE 2 – Centrifugal load:** the contribution of the resistant torque of the struts was again
239 not considered but a limitation on the centrifugal stress acting on the blades was added as a
240 function of the rotational speed of each model.

241 ▪ **CASE 3 – Struts’ parasitic torque:** in this latter configuration, both a limitation on the
242 centrifugal stress on the blades and variable struts dimensions, as a function of the
243 rotational speed of each model, were included. Moreover, the resistant torque of the struts
244 was taken into account.

245 In order to give a correct estimation of the structural loads, in this study a manufacturing
246 technology based on extruded aluminium blades with a hollowed section was considered,
247 utilizing real data on both the maximum centrifugal stress and on the maximum mechanical
248 stress on the struts available from previous design experiences of the authors [33].

249 In further detail, in Case 2 the cut-out speed of the turbine was calculated in each case-study
250 based on the hypothesis that the maximum centrifugal stress at the middle of the blade (where

251 the maximum displacement is located) would not exceed a fixed stress limit of the blade itself
252 (Eq. 6).

$$253 \quad \zeta_b = \frac{F_b}{A_{res_b}} = \frac{m_b \omega^2 R}{A_{res_b}} \leq \zeta_{lim_b} \quad (6)$$

254 where A_{res_b} is a conventional resistance area which takes into account the structure of the
255 stiffeners inside the airfoil and F_b is the centrifugal stress of the blade of mass m_b . In particular,
256 all the airfoils were reproduced with a hollowed section having a constant skin thickness (3
257 mm) and three, equally spaced, rectangular stiffeners perpendicular to the chord of variable
258 thickness. The trailing edge was considered as solid with a filet radius increasing proportionally
259 to the chord of the blade (Figure 3). Based on the characteristics of an aluminium alloy tested
260 by the authors in a previous industrial experience [33,37], a stress limit of 90 N/mm² was here
261 considered.

262 In addition, in Case 3 even the dimensions of the struts (at least two for each blade) are
263 variable from one configuration to another in order to satisfy the stress limit of the blades due
264 to the centrifugal force (Eq. 7 with the same notation of Eq. 6).

$$265 \quad \zeta_{ST} = \frac{F_{ST}}{A_{res_ST}} = \frac{1}{N_{ST}} \frac{m_b \omega^2 R}{A_{res_ST}} \leq \zeta_{lim_ST} \quad (7)$$

266 It is worth pointing out that the load case considered in Eq. 7 takes into account only the
267 tensile stresses generated by the centripetal acceleration of the rotor. In authors' experience
268 (see [33,37]), this load condition is quite realistic for small-size rotors (i.e. with a swept area up
269 to 4.0 m²), whereas bending forces become significant in larger rotors with high Φ ratios. In
270 this work, the bending stresses were neglected but a more accurate description of their
271 influence will be carried out in future works.

272 A correct evaluation of the strut's dimensions is particularly important in small rotors due to
273 the fact that a fast-rotating turbine often needs thick supporting struts to balance the centrifugal

274 stresses [24]. Similar struts, however, are characterized by a notable parasitic torque generation
275 which causes a remarkable detriment of the overall performance of the machine.

276 In particular, in this study a constant shape of the struts was considered. In case of
277 symmetrical airfoils, the same profiles were used. On the other hand, when the NACA4415 is
278 used, the struts are supposed to be realized with the NACA0015 (same t/c ratio but straight
279 camber). By these choices, a constant virtual drag coefficient [24] during the revolution was
280 considered, whereas the dimensions of the struts were varied in Case 3 until the minimum ones
281 which satisfied Eq. 7 were found. In detail, the chord of the struts (and consequently also the
282 thickness, being the t/c ratio fixed) was calculated on the basis of the resistant area defined by
283 Eq.7. When the calculated struts dimensions exceeded the chord of the blade, the struts number
284 was increased by one for each blade and the new dimensions of each element were re-
285 calculated on the basis of the same procedure, in all the investigated configuration, a maximum
286 struts' number of three was constantly observed. Finally, the effects of "bluff-section" struts
287 was investigated, in order to stress more evidently the influence of the parasitic phenomena: the
288 struts were assumed to have a constant virtual drag of 0.3 and a thickness varying with the
289 same procedure described for the airfoil-shaped solutions.

290 **4. Simulations and data reduction**

291 The performance simulations of the machines were carried out with the *VARDAR* code of the
292 Department of Industrial Engineering of the University of Florence. The code makes use of the
293 Blade Element Momentum (BEM) Theory, by which the rotor performance is calculated
294 coupling the momentum equation in the mainstream direction of the wind and a one-
295 dimensional aerodynamic analysis of the interactions between the airfoils in motion and the
296 oncoming flow on the rotor [20,33,38-39] by means of pre-calculated polars. Even if more
297 advanced simulations techniques (including computational fluid dynamics) are today available
298 for the simulation of VAWTs (e.g. [39-41]), BEM approaches are still the most widely
299 exploited tools for the preliminary design of these rotors, as they provide sufficiently reliable

300 results in terms of global performance (whereas a poor description of the instantaneous flow
 301 field around the rotor is achieved) coupled with a notably reduced computational cost.

302 In particular, the VARDAR code has been specifically developed for H-Darrieus wind
 303 turbines using an improved version of a *Double Multiple Streamtubes Approach with Variable*
 304 *Interference Factors* [17,28,42] (Figure 4a). In this approach, the elementary torque for each
 305 azimuthal position is therefore given by Eq. 8:

$$306 \quad T_{blade}(\vartheta) = F_t \cdot R = \frac{1}{2} \rho c W_{\vartheta}^2 C_{t(\vartheta)} R H \quad (8)$$

307 where C_t and W represent the tangential coefficient of the airfoil in the reference system of the
 308 rotating blade (Figure 4b) and the relative velocity of the flow experienced by the airfoil itself
 309 in the upwind or downwind half, respectively, expressed by Eqs. 9,10 and 11:

$$310 \quad C_t = C_L \cdot \sin \alpha - C_D \cdot \cos \alpha \quad (9)$$

$$311 \quad W_{up} = \sqrt{[(1-a) \cdot U_{\infty} \cdot \sin(\vartheta - \beta)]^2 + [(1-a) \cdot U_{\infty} \cos(\vartheta - \beta) + \omega R]^2} \quad (10)$$

$$312 \quad W_{down} = \sqrt{[(1-a_2) \cdot U_{eq} \cdot \sin(\vartheta - \beta)]^2 + [(1-a_2) \cdot U_{eq} \cos(\vartheta - \beta) + \omega R]^2} \quad (11)$$

313 As for the more general Eq. 5, the relative speed is given by the sum of peripheral speed and
 314 wind speed, properly reduced by the induction factor (either upwind or downwind). The value
 315 U_{eq} in Eq. 25 indeed represents the wind equilibrium velocity between actuator disks (see
 316 Figure 4).

317 The Glauert's correction for the BEM theory has been taken into account with the most recent
 318 improvements, together with the corrections due to blades finite Aspect Ratio, using the
 319 Lanchester-Prandtl model. This aspect is of particular relevance in the present analysis, as it
 320 allows the designer to account for the increasing tip-losses connected to blades with small
 321 height to chord ratios.

322 In order to increase the accuracy of the aerodynamic estimations, a specific sub model to
 323 account for the dynamic stall has been provided, following the Paraschivoiu's adaptation to the

324 DMS approach described in; at the same time, the stream tube expansion along the flow path
 325 was considered. For additional details on the code please refer to Refs. [23,26,33,37,42-43].

326 The prediction capabilities of the VARDAR code have been validated during a several-years'
 327 experience in the design of three real H-Darrieus rotors, having swept areas of 1, 2.5 and 5 m²,
 328 respectively, and two or three blades, either straight or helix-shaped. The 1:1 models of all the
 329 rotors (two made of reinforce plastic and one of painted aluminium alloy) were tested in
 330 different wind tunnels (both with closed and open-jet). In all cases, the code was able to
 331 correctly predict both the power curves at different wind speeds and the starting ramps of rotor
 332 and is then considered fully predictive for the turbine typology investigated in this study. For
 333 further details on the code validation please refer to Refs. [23,33,37,42].

334 In the present analysis, the code provided the power coefficient of each configuration at all
 335 the wind speeds between the cut-in and the cut-out. The characteristic power coefficient of the
 336 machines at each wind velocity was conservatively evaluated in correspondence with the
 337 calculated performance 0.2 points of TSR after the peak of the operating curve. A similar
 338 precaution is often applied in order to define a load curve aimed at preventing the turbine from
 339 operating in the unstable part of the functioning curve [11,24]. Moreover, it is worth noticing
 340 that the cut-in speed in each case was set to the wind speed for which a positive power
 341 coefficient is obtained. This is, in fact, a precautionary assumption, because the self-starting of
 342 an H-Darrieus rotor in real wind is often ensured for several starting positions even if the
 343 overall power coefficient over the revolution is negative [42,45].

344 In further detail, for each configuration in terms of swept area (i.e. the discrete variable of the
 345 problem) specific performance maps were created [26] corresponding to a given wind
 346 distribution. Each map (e.g. see Figure 5) contains the overall efficiency of energy conversion
 347 (η_{en}) of the specific rotor, defined as in Eq. 12 and 13.

$$348 \quad \eta_{en} = \frac{\sum_{u=cut-in}^{cut-out} c_p(u) \cdot u^3 \cdot T(u)}{\sum_{u=cut-in}^{cut-out} u^3 \cdot T(u)} \quad (12)$$

349
$$T(u) = f(u) \cdot 8760 \quad (13)$$

350 Upon examination of the equations, it is worth pointing out that the energy conversion
351 efficiency was defined as the annual energy yield of the turbine over the year (i.e. the real
352 extracted power at each wind speed multiplied by the time fraction, in hours, during which that
353 wind blows $T(u)$) on the theoretical energy contained in the wind itself.

354 Based on its definition, this indicator differs from the classical power coefficient and allows
355 one to simultaneously take into account both the efficiency of the turbine at all the wind speeds
356 expected over the year and the effects related to the starting and resistance capabilities of the
357 rotor (due to the variable cut-in and cut-out velocities considered).

358 Finally, within each map, a numerical identification of the maximum was performed, with the
359 constraints of neglecting design solutions which imply Blade's Aspect Ratios higher than 35: in
360 case of excessive ratios between the height and the chord, the bending resistance of such a
361 slender blade would be indeed very poor, making the selected solution practically unfeasible.

362 This procedure would finally lead to the definition of the geometrical features of the rotor
363 ensuring the largest energy harvesting over a year for the attended load case, average wind
364 speed in the site and imposed swept area of the rotor.

365 The whole data reduction procedure is summarized in Figure 6, while a complete overview on
366 the results in terms of best design solutions can be find in the Appendix Section.

367 **5. Results**

368 **5.1 Energy Efficiency maps interpretation**

369 A typical Energy Efficiency map has been presented in Figure 5 (e.g. for a swept area of 4.0
370 m^2 , NACA0018 airfoil, $\bar{U}=5$ m/s in Case 2). A linear interpolation was performed between the
371 calculated points (see Table 1) in order to more precisely outline the contours.

372 It is readily noticeable that an optimum-design zone (white-colored in the figure) can be
373 typically distinguished in the bottom side. This zone represents the combination of the Φ and ζ

374 parameters which ensures the best compromise in terms of functioning Reynolds numbers on
375 the airfoil (high peripheral speeds and chords) and efficiency of the blades (high Aspect
376 Ratios). Moreover, one can also notice that the efficiency is almost zero in the left side of the
377 map, where the very small chords remarkably reduce the lift generation, and becomes lower
378 also in the right-bottom corner of the map, where the turbine heights tend to zero.

379 As discussed, within each map a numerical identification of the maximum was performed in
380 order to define the geometrical features of the rotor ensuring the largest energy harvesting over
381 a year under the present design constraints.

382 **5.2 Case 1 - Aerodynamics**

383 From a general point of view, it is worth remembering that Case 1 configuration actually
384 refers to a hypothetical solution of a fully aerodynamic relationship between the geometrical
385 features of the rotor and the power performance. By doing so, the influence of the main
386 aerodynamic design parameters can be readily argued and the functioning behaviors of
387 machines having different areas can be directly compared.

388 The main outcome of the analysis of Case 1 is that an opposite behavior was found between
389 cambered and uncambered airfoils in this configuration.

390 As an example of uncambered airfoils, Figure 7 reports the variation trends which describe
391 the dependence of the optimal values of the most relevant design parameters from the average
392 wind speed for the NACA0015 airfoil.

393 Upon examination of Figure 7, some relevant markups can be promptly made. In particular:

- 394 ■ The dimensionless parameters present the same trends even when different swept areas are
395 considered, although numerical values differ from one configuration to another,
396 confirming that scale effects must be taken into account.
- 397 ■ When the average wind speed in the site increases, the best solidity decreases constantly
398 and the Aspect Ratio rises significantly, whereas the Shape Factor Φ increases for

399 medium-low average wind speeds and then becomes stable. As a general remark, however,
400 the turbine tends to become slenderer by increasing the average wind speed.

401 ■ Focusing on the dimensional parameters, the aforementioned trend is basically obtained
402 throughout a constant decrease of the blades' chord with the average wind speed increase
403 (with a steeper trend for medium-low \bar{U} and a flatter trend with an increased \bar{U}). The
404 turbine diameter and height have instead an opposite trend, with a decrease and an increase
405 in the first part, respectively, followed by a constant trend in the second part.

406 The main aerodynamic implication of these results is that, when the average wind velocity
407 experienced by the turbine is low (left side of the plots), the best design is that ensuring the
408 highest local Reynolds numbers on the blade by means of the geometrical proportions. As a
409 consequence, the chord values are maximized (see Eq. 1) at low wind speeds and then the
410 solidity values are high (Eq. 3).

411 By increasing the average wind speed, the velocity triangles on the airfoils are altered thanks
412 to the increased relative velocities experienced by the blades: the chords can be therefore
413 reduced without decreasing the functioning Reynolds numbers. For high mean wind velocities,
414 however, the chord length stops decreasing and more efficient blades (i.e. higher Aspect Ratios,
415 $AR=H/c$ [20-21,24]) are obtained by means of an increase of the turbine height (black curves in
416 the graphs on the left). The optimal solidity constantly decreases with \bar{U} .

417 Moreover, a well-defined dependence on the t/c ratio of the airfoil was observed. For
418 example, in Figures 7 and 8 the optimal trends of the solidity and the blade's Aspect Ratio for
419 the three uncambered airfoils are reported.

420 In detail, by decreasing the t/c ratio of the selected airfoil (Figure 8), i.e. from NACA0018 to
421 NACA0015 and NACA0012, the optimal solidity of the turbine is constantly reduced. This
422 phenomenon can be related to a decrease of the requested chord. This solution is indeed
423 allowed by an increase of the target peripheral speed of the rotor which, on one hand, ensure a
424 suitable Reynolds number on the airfoil (Eq.1) and, on the other hand, decreases the incidence

425 angles range: thinner airfoils (e.g. the NACA0012), although more efficient for high relative
426 speeds, have indeed a lower stall angle and are generally more sensitive to incidence angle
427 variations. Contemporarily (Figure 9), the same reasons induce an opposite behavior of the
428 blade's Aspect Ratio (AR_b), which is constantly higher in case of thinner airfoils (the shorter
429 chords are combined with an almost equal trend of optimal heights).

430 The optimal design trends in case of the cambered NACA4415 airfoil are notably different. In
431 particular, whenever this typology of profile is applied, the scale effects due to the swept area
432 become negligible, as the high C_L/C_D ratio of this airfoil [44] makes the dependence of the
433 aerodynamic performance from the chord very low. The Aspect Ratio can then rise
434 significantly to pursue the higher blade's efficiency. The optimal design proportions in Case 1
435 for the NACA4415 airfoil are reported in Figure 10. In this configuration, the optimal solidity
436 is low (see Eq. 3) and the AR_b very high mainly due to the very short chords.

437 **5.3 Case 2 - Limited centrifugal load**

438 The results obtained from the examination of Case 1 are very useful to comprehend the
439 aerodynamic trends connected to a variation of the wind velocities experienced by the turbine;
440 structural constraints like the centrifugal load have, however, relevant impact on the best design
441 compromise of a machine [24,26].

442 To this purpose, next figures report some results of the investigation on the study-cases in
443 Case 2, in which a $\zeta_{lim,b}$ (Eq. 6) of 90 N/mm^2 was considered [26,33]; for a wider overview of
444 the results, please see Appendix B.

445 First, it was noticed that, when the average wind velocities are low (i.e. $3\div 4 \text{ m/s}$), the
446 structural constraints actually do not affect the definition of the best design parameters; the
447 operating rotational speeds at these velocities are low and the resulting centrifugal loads do not
448 exceed the structural limits. In case of the NACA4415, the best design is once again imposed
449 due to limitation on the blade's Aspect Ratio.

450 Once again, the two types of airfoils work differently. If the uncambered profiles are selected
451 and the medium-high wind speeds become more frequent, the reduction of the solidity with the
452 average wind speed noticed in Case 1 ceases (an almost constant value is reached – e.g. see
453 Figure 11), mainly due to the stop in the decrease of the optimal chord (Figure 12).

454 This trend can be explained by considering that, when the wind velocities are high, the most
455 suitable compromise in terms of energy-yield capabilities comes from a reduction of the peak
456 efficiency of the turbine (higher solidity) which, however, implies a reduction of the operating
457 rotational regime [24,26]. This reduction makes the centrifugal loads decrease and allows the
458 turbine to extract energy from the wind with all the considered wind velocities.

459 In particular, after examining the Energy Efficiency maps (e.g. for the NACA0018, swept
460 area $A=4 \text{ m}^2$ in Figure 13), it is readily noticeable that, for low average wind speeds, the best
461 efficiency zone first migrates towards lower solidities and higher Φ ratios. When the high wind
462 speeds become more frequent, however, a new zone of best efficiency arises at higher ζ and Φ
463 ratios.

464 On the other hand, in case the NACA4415 is adopted, the optimal design solution highlighted
465 in Case 1 (small chords, very high AR_b and high revolution speeds) is no longer feasible due to
466 the limitation to the centrifugal load.

467 As a result, the best solidity value is slightly increased for medium-high average wind speeds
468 (Figure 14); contemporarily, the chords and diameters remarkably increase in order to achieve
469 a drastic reduction of the revolution speed (Figure 15). One should indeed remember that
470 longer chords ensure more favorable Reynolds numbers on the airfoil without increasing the
471 relative speed (see Eq. 3), whereas higher diameters act oppositely by improving the relative
472 speed (Eq. 4) or, conversely, ensure the same relative speed with lower revolution speeds.

473 Finally, it is also worth noticing that this increase of the diameter for high average wind speeds
474 is avoided only for high swept areas (i.e. $A=9.0 \text{ m}^2$), where the limit on the centrifugal load is

475 mitigated by the large diameters. In these conditions, the AR_b can be also slightly increased,
476 with a partial recovery of the blades' efficiency (see Appendix B).

477 **5.4 Case 3 - Centrifugal load and struts' parasitic torque**

478 Focusing now on a real-type machine, a further constraint must be included in the
479 identification of the best design trends: the parasitic torque of the struts is, in fact, a key
480 element in defining both the peak efficiency of the machine and its functioning behaviour at
481 different wind speeds. Due to the relevance of this load case, the complete comparison of the
482 optimal design configurations was reported in Appendix D.

483 The calculations showed that the general effect of the parasitic torque is to slightly flatten the
484 trends of the design parameters as a function of the average wind speed. The best design
485 solutions tend in fact to collapse in the configurations that minimize the contribution of the
486 parasitic components [26]. The general tendencies described in Section 4.3 are, however, still
487 of validity and will not be all again discussed. In particular, the efficiency maps shape
488 discussed in Figure 13 was confirmed also under this load case, with the only discussed
489 restriction of the high-efficiency zone. Some interesting remarks can however be made.

490 First, Figure 16 reports the comparison between the optimal solidity trends in Case 2 and 3 for
491 NACA0012 and NACA0018 airfoils (swept area of 1.0 m^2), as a function of the average wind
492 speed. As one may notice, no great difference stands between the two cases when the average
493 wind speed in the site is sufficiently high (i.e. higher than 5 m/s). Conversely, in case of low
494 average wind speeds, the optimal solidity in Case 3 is higher than that obtained in case the
495 parasitic torque is neglected.

496 In order to give a correct interpretation of the results, it is worth remembering that the
497 parasitic torque generated by the rotating structures which do not contribute to the torque
498 generation (e.g. struts, tie-rods, etc.), has a quadratic dependence on the rotational speed of the
499 rotor (directly affecting the tangential velocity) and a lighter and more complex dependence on
500 the wind velocity (see Refs. [33,36]).

501 Based on these considerations, one can understand that, when the wind speeds are low, the
502 impact of the parasitic torque on the effective energy-extraction capability of the rotor is more
503 relevant: as a consequence, the optimal design tends to increase the solidity, in order to achieve
504 a reduction of the revolution regime [24].

505 Focusing on the cambered airfoil, the situation is again quite different (see Figure 17). With
506 this airfoil selection, which is thought to provide a good torque production even in low winds,
507 the best design solution is almost unaltered within $\bar{U}=5$ m/s with respect to Case 2.

508 When the high wind speeds in the site become more frequent, however, the “low solidity”
509 solutions, which are associated with very high revolution speeds, are not suitable anymore, as
510 the parasitic torque has become too high. The optimal solutions hence tend to higher solidities
511 (i.e. slower revolution speeds), very similar to those identified for the uncambered airfoils.

512 Finally, in order to further stress the importance of the parasite torque of the struts, in Figure
513 18 a comparison between the optimal solidity for a turbine with the NACA0012 airfoil and a
514 swept area of 1 m^2 is reported as a function of the strut’s shape. In detail, when the drag of the
515 struts increases, the solidity tends to notably increase, in the attempt of reducing the revolution
516 speed of the rotor. In the selected case, the more energy-efficient solution would be very solid
517 (even up to the limit of $\sigma = 0.6$), which is, however, a practically unfeasible solution. In a
518 similar case, a compromise must be pursued in practically designing the rotor, including a
519 reduction of the effective energy-yield capabilities.

520 At the end of this study, one could then conclude that, from an energy viewpoint, future
521 design of medium and small-size Darrieus rotors should be based on the maximization of the
522 energy yield on the basis of the characteristics of the potential installation site. In particular, for
523 given rotor’s dimensions, a differently shaped turbine would be about to be preferred as a
524 function of the average wind speed of the installation. For example, in Figure 19 the optimal
525 design choices for a turbine having a swept area of 4 m^2 and equipped with NACA0018 airfoils
526 are presented as a function of the average wind speed in the site. In particular, the

527 [aforementioned trends in terms of increase of the H/D ratio and decrease of the chord length](#)
528 [are clearly distinguishable.](#)

529 For the same family of turbines (presented trends are consistent with all the analyses
530 presented in this study), the annual energy yield of the optimized rotors is presented in Figure
531 20 as a function of the average wind speed in the site. In order to provide a sensitivity analysis
532 on the benefits of the proposed approach, in the same figure the energy yield increase with
533 respect to two others design choices is presented. In further details, Study Turbine A represents
534 a hypothetical turbine designed to have the maximum efficiency at 6 m/s, which could be, for
535 example, the average speed in the site [23]. Study Turbine B instead represents the turbine
536 optimized by means of the maximum-energy-yield criterion at $\bar{U}=6$ m/s.

537 Some very interesting remarks can be done. First, it is worth noticing that a design approach
538 based on the maximum annual energy yield actually provides an increase of performance in all
539 cases. In particular, focusing on the 6 m/s bar, one can notice that benefits can be achieved also
540 in comparison to a design criterion based on the same average speed of the site.

541 Moreover, the proposed criterion is able to provide notable energy increase (up to 10% in the
542 present case) when the wind speeds in the site are low, confirming the prospects of specific
543 future design choices for these conditions.

544 **6. Conclusions**

545 In this study, a numerical analysis has been carried out to define some design guidelines for
546 Darrieus wind turbines aimed at optimizing the annual energy yield of each machine in the
547 installation site. The main outcomes of the analysis can be summarized as follows.

548 Focusing on the only aerodynamic requirements, an opposite behavior was found between
549 cambered and symmetric, uncambered airfoils. For uncambered profiles, when the average
550 wind speed in the site increases, the best solidity decreases constantly, the Aspect Ratio rises
551 significantly, whereas the Shape Factor Φ increases for medium-low average wind speeds and
552 then becomes stable. This trend is mainly due to the fact that, by increasing the wind speed, the

553 relative velocity is increased, and the Reynolds number is improved. The chords can be then
554 reduced, with notable benefits in terms of blade's efficiency. A well-defined dependence on the
555 t/c ratio was also observed: by decreasing the t/c ratio, the optimal solidity is constantly lower
556 whereas higher Aspect Ratios are preferable. When a cambered airfoil is instead selected, the
557 scale effects due to the swept area becomes negligible, as the high C_L/C_D ratio of this airfoil
558 makes the dependence of the aerodynamic performance from the chord very low, hence
559 allowing the Aspect Ratio to rise significantly to pursue the higher blade's efficiency. With this
560 selection, the optimal solidity is consequently also very low.

561 On the other hand, when structural constraints and notable parasitic contributions are
562 introduced, the best configurations when the average wind velocities are low are similar to that
563 coming from the aerodynamic analysis, although the optimal design generally tends to increase
564 the solidity, in order to ensure a better functioning conditions to the airfoils (higher Reynolds
565 numbers, increased torque) and contemporarily achieve a reduction of the revolution regime,
566 which contains the parasitic torque. On the other hand, when the medium-high wind speeds
567 become more frequent, the most suitable compromise in terms of energy-yield capabilities
568 generally comes from a reduction of the peak efficiency of the turbine which, however, ensures
569 a good energy extraction is a wider range of functioning conditions. In case of uncambered
570 airfoils, in particular, this goal is obtained with a general increase of the optimal solidity, which
571 makes the revolution speed decrease and allows the turbine to extract energy from the wind
572 with all the considered wind velocities. As a general remark, however, by increasing the
573 parasitic contributions, the transition of the best design compromise to higher solidity solutions
574 is anticipated, due to the stronger dependence of the performance on the rotational speed.

575 At the end of this work, it has to be noticed that the present analysis was carried out under
576 specific assumptions in terms of dimensions, airfoil types, load system and struts' shape; on
577 these bases, the reader has to consider that different performance maps could come from a new
578 set of theoretical assumptions, although some general trends outlined in the work (e.g. the

579 influence of the turbine proportions on the Reynolds numbers and the rotational speed) are of
580 general validity.

581 The proposed design criterion, however, besides being theoretically more rigorous from a
582 truly energetic point-of-view than a conventional one based on a single reference wind speed,
583 has shown interesting prospects in terms of energy production improving. In particular,
584 different models could be designed for specific wind distributions in order to optimize the
585 energy yield also at low wind speeds, which are very frequent in several countries and in
586 unconventional installation sites, e.g. the urban environment.

587 **Nomenclature**

588	A	Swept Area	$[\text{m}^2]$
589	a	Induction Factor	
590	AR	Aspect Ratio	
591	c	Blade Chord	$[\text{m}]$
592	C_D	Drag Coefficient	
593	C_L	Lift Coefficient	
594	C_t	Tangential Force Coefficient	
595	c_P	Power Coefficient	
596	D	Turbine Diameter	$[\text{m}]$
597	F_n	Normal Force on the Blade	$[\text{N}]$
598	F_{ST}	Force due to Centrifugal Loads	$[\text{N}]$
599	F_t	Tangential Force on the Blade	$[\text{N}]$
600	f	Frequency	
601	H	Turbine Height	$[\text{m}]$
602	m	Mass	$[\text{kg}]$
603	N	Blades/Struts Number	
604	P	Power	$[\text{W}]$

605	R	Turbine Radius	[m]
606	Re_c	Chord-based Reynolds Number	
607	T	Annual Time of each Wind Class	[h]
608	t	Airfoil Thickness	[m]
609	TSR	Tip-Speed Ratio	
610	u	Wind Class	[m/s]
611	U_∞	Absolute Wind Speed	[m/s]
612	\bar{U}	Average Wind Speed	[m/s]
613	W	Relative Wind Speed	[m/s]
614			
615	<u>Superscripts</u>		
616	*	Per Unit Area	
617	\rightarrow	Vectorial Quantity	
618			
619	<u>Subscripts</u>		
620	air	Air	
621	b	Blade	
622	en	Energy	
623	eq	Equilibrium (between upwind and downwind)	
624	res	Resistant Component	
625	ST	Struts	
626			
627	<u>Greek letters</u>		
628	Φ	Turbine Shape Factor	
629	α	Incidence Angle on the Airfoils	[deg]
630	β	Pitch Angle	[deg]
631	η_{en}	Energy-conversion Efficiency	

632	ν	Kinematic Viscosity	$[\text{m}^2/\text{s}]$
633	ζ	Chord/Diameter Ratio	
634	ρ	Air Density	$[\text{kg}/\text{m}^3]$
635	σ	Solidity	
636	ς	Structural Stress	$[\text{N}/\text{m}^2]$
637	ω	Rotational Speed	$[\text{rad}/\text{s}]$

638 **References**

- 639 [1] Global Wind Report. Global Wind Energy Council; 2011.
- 640 [2] Global Wind Energy Outlook. GWEC, Brussels (Belgium); 2011.
- 641 [3] Oceans of Opportunity. EWEA, Brussels (Belgium); 2009.
- 642 [4] Junginger M, Faaij A, Turkenburg WC. Cost Reduction Prospects for Offshore Wind
643 Farms. *Wind Engineering* 2004;28(1):97–118.
- 644 [5] Kirke BK, Evaluation of self-starting vertical axis wind turbines for standalone
645 applications. Ph.D. thesis, Griffith University, Gold Coast (Australia); 1998.
- 646 [6] Small Wind Turbine Global Market Study. AWEA, Whashington DC (USA); 2008.
- 647 [7] Mertens S. *Wind Energy in the Built Environment*. Brentwood (UK): Multi-Science; 2006.
- 648 [8] Dayan E. Wind energy in buildings: Power generation from wind in the urban environment
649 - where it is needed most. *Refocus* 2006;72(2):33-38.
- 650 [9] Beller C. *Urban Wind Energy - State of the Art 2009*, Risø Laboratory - DTU, Roskilde
651 (Denmark), Tech. rep. Risø-R-1668(EN); 2009.
- 652 [10] Balduzzi F, Bianchini A, Ferrari L. Microeolic turbines in the built environment: influence
653 of the installation site on the potential energy yield. *Renewable Energy* 2012;45:163-174.
- 654 [11] Balduzzi F, Bianchini A, Carnevale EA, Ferrari L, Magnani S. Feasibility analysis of a
655 Darrieus vertical-axis wind turbine installation in the rooftop of a building. *Applied Energy*
656 2012;97:921–929.

- 657 [12] Syngellakis K. Urban wind turbines: Development of the UK market. Proc. of the
658 European Wind Energy Conference 2006, February 27-March 2, Athens (Greece); 2006.
- 659 [13] Banks D, Cochran B, Denoon R., Wood G. Harvesting Wind Power from Tall Buildings.
660 Proc. of the CTBUH 8th World Congress, Dubai (UAE), 2008 In: Chicago: Council on Tall
661 Buildings and Urban Habitat; 2008, pp. 320-327.
- 662 [14] Sarma NK, Biswas A, Misra RD. Experimental and computational evaluation of Savonius
663 hydrokinetic turbine for low velocity condition with comparison to Savonius wind turbine at
664 the same input power. Energy Conversion and Management 2014;83:88-98.
- 665 [15] Roy S, Saha UK. Review of experimental investigations into the design, performance and
666 optimization of the Savonius rotor. Proc. of the Institution of Mechanical Engineers, Part A:
667 Journal of Power and Energy 2013;227(4):528-542.
- 668 [16] Gupta R, Biswas A, Sharma KK, Comparative study of a three-bucket Savonius rotor with
669 a combined three-bucket Savonius-three-bladed Darrieus rotor. Renewable Energy 2008;33(9):
670 1974-1981.
- 671 [17] Mertens S, van Kuik G, van Bussel G. Performance of an H-Darrieus in the Skewed Flow
672 on a Roof. Journal of Solar Energy Engineering 2003;125:433-440.
- 673 [18] Simão Ferreira CJ, van Bussel G, van Kuik G. An analytical method to predict the
674 variation in performance of a H-Darrieus in skewed flow and its experimental validation. Proc.
675 of the European Wind Energy Conference, February 27-March 2, 2006, Athens (Greece); 2006.
- 676 [19] Bianchini A, Ferrara G, Ferrari L, Magnani S, An improved model for the performance
677 estimation of an H-Darrieus wind turbine in skewed flow. Wind Engineering 2012;36(6):667-
678 686.
- 679 [20] Paraschivoiu I, Wind Turbine Design with Emphasis on Darrieus Concept. Polytechnic
680 International Press, Canada; 2002.

681 [21] Bianchini A, Ferrari L, Magnani S. Analysis of the Influence of Blade Design on the
682 Performance of an H-Darrieus Wind Turbine. Proc. ASME-ATI-UIT 2010 Conference on
683 Thermal and Environmental Issues in Energy Systems, Sorrento (Italy) May 16-18; 2010.

684 [22] Sharpe T, Proven G. Crossflex: Concept and early development of a true building
685 integrated wind turbine. *Energy and Buildings* 2010;42:2365-2375.

686 [23] Bianchini A, Ferrari L, Schneider A. First steps in the design and optimization of Darrieus
687 VAWTs for microeolic applications. Proc. World Renewable Energy Congress (WREC) X,
688 Glasgow (Scotland), July 19-25; 2008.

689 [24] Ferrari L, Bianchini A. Critical aspects in the design of a small-size Darrieus wind turbine.
690 Proc. World Renewable Energy Congress (WREC) XI, Abu Dhabi (UAE) September 25-30;
691 2010.

692 [25] Aslam Bhutta MM, Hayat N, Farooq AU, Ali Z, Jamil ShR, Hussain Z, Vertical axis wind
693 turbine – A review of various configurations and design techniques. *Renewable and*
694 *Sustainable Energy Reviews* 2012;16(4):1926-1939.

695 [26] Bianchini A, Ferrari L, Magnani S. Energy-yield-based optimization of an H-Darrieus
696 wind turbine. Proceedings of the ASME Turbo Expo 2012, Copenhagen (Denmark), June 11-
697 15; 2012.

698 [27] Manwell JF, McGowan JG, Rogers AL. *Wind Energy Explained*, 2nd edition, Wiley,
699 U.K.; 2009.

700 [28] Justus CG, Hargraves WR, Mikhail A, Graber D. Methods for estimating wind speed
701 frequency distributions. *Journal of Applied Meteorology* 1978;17(3):350-353.

702 [29] Akdağ SA, Dinler A. A new method to estimate Weibull parameters for wind energy
703 applications. *Energy Conversion and Management* 2009;50(7):1761-1766.

704 [30] Freitas de Andrade C, Maia Neto HF, Costa Rocha PA, Vieira da Silva ME. An efficiency
705 comparison of numerical methods for determining Weibull parameters for wind energy

706 applications: A new approach applied to the northeast region of Brazil. *Energy Conversion and*
707 *Management* 2014;86(10):801-808.

708 [31] Bhuyan S, Biswas A. Investigation on self-starting and performance characteristics of
709 simple h and hybrid H-Savonius vertical axis wind rotors. *Energy Conversion and Management*
710 2014;87:859-867.

711 [32] Gupta R, Das R, Sharma KK. Experimental study of a Savonius-Darrieus wind machine.
712 In *Proceedings of the International Conference on Renewable Energy for Developing*
713 *Countries*, University of Columbia, Washington DC, 2006.

714 [33] Bianchini A. Performance Analysis and Optimization of a Darrieus VAWT. PhD Thesis,
715 School of Energy Engineering and Innovative Industrial Technologies, University of Florence
716 (Italy); 2011.

717 [34] Islam M, Ting D, Fartaj A, Desirable Airfoil Features for Smaller-Capacity Straight-
718 Bladed VAWT. *Wind Engineering* 2007;31(3):165–196.

719 [35] Klimas PC. Tailored Airfoils for Vertical Axis Wind Turbines. Sandia National
720 Laboratories, Albuquerque, N.M., SAND 84-1062; 1984.

721 [36] Paraschivoiu I, Delclaux F. Double Multiple Streamtube Model with Recent
722 Improvements. *Journal of Energy* 1983;7(3):250-255.

723 [37] Balduzzi F, Bianchini A, Maleci R, Ferrara G, Ferrari L. Blade design criteria to
724 compensate the flow curvature effects in H-Darrieus wind turbines. *Journal of Turbomachinery*
725 2015;137(1):1-10.

726 [38] Camporeale SM, Magi V. Streamtube model for analysis of vertical axis variable pitch
727 turbine for marine currents energy conversion. *Energy conversion and Management*
728 2000;41(16):1811-1827

729 [39] Islam M, Ting D SK, Fartaj A. Aerodynamic models for Darrieus-type straight-bladed
730 vertical axis wind turbines. *Renewable and Sustainable Energy Reviews* 2008;12:1087-1109.

- 731 [40] Wang LB, Zhang L, Zeng ND. A potential flow 2-D vortex panel model: Applications to
732 vertical axis straight blade tidal turbine. *Energy Conversion and Management* 2007;4(2):454-
733 461.
- 734 [41] Simão Ferreira CJ. The near wake of the VAWT: 2D and 3D views of the VAWT
735 aerodynamics. PhD Thesis, Technische Universiteit Delft, The Netherlands, 2009.
- 736 [42] Bianchini A, Ferrari L, Magnani S. Start-up behavior of a three-bladed H-Darrieus
737 VAWT: experimental and numerical analysis. Proc. of the ASME Turbo Expo 2011,
738 Vancouver (Canada), June 6-10; 2011.
- 739 [43] Bianchini A, Ferrari L, Carnevale E.A.. A model to account for the Virtual Camber Effect
740 in the Performance Prediction of an H-Darrieus VAWT Using the Momentum Models. *Wind*
741 *Engineering* 2011;35(4):465-482.
- 742 [44] Ostowari C, Naik D. Post stall studies of untwisted varying aspect ratio blades with an
743 NACA 4415 airfoil section - Part I. *Wind Engineering* 1984;8(3):176-194.
- 744 [45] Dominy R, Lunt P, Bickerdyke A, Dominy J. Self-starting capability of a Darrieus turbine.
745 Proc. IMechE 221 Part A: Journal of Power and Energy 2007:111-120.